Contrib Mineral Petrol (2009) 158:197–222
DOI 10.1007/s00410-009-0378-5

ORIGINAL PAPER

Insights into Li and Li isotope cycling and sub-arc metasomatism from veined mantle xenoliths, Kamchatka

Ralf Halama · Ivan P. Savov · Roberta L. Rudnick · William F. McDonough

Received: 3 July 2008 / Accepted: 7 January 2009 / Published online: 30 January 2009

Abstract Harzburgitic xenoliths cut by pyroxenite veins from Avachinsky volcano, Kamchatka, are derived from the sub-arc mantle and record element transfer from the slab to the arc. Olivine and orthopyroxene in the harzburgites have Li isotopic compositions (δ^7Li = +2.8 to +5.6) comparable to estimates of the upper mantle (δ^7Li ~ +4 ± 2). The pyroxenite veins, which represent modal metasomatism and may therefore provide information about the metasomatic agent, have mantle-normalized trace element characteristics that suggest overprinting of their mantle source by an aqueous, slab-derived fluid. These include relative enrichments of Pb over Ce, U over Th and Sr over Nd. Li is enriched relative to the HREE, and ortho- and clinopyroxene from the veins are in Li elemental and isotopic equilibrium with each other and the surrounding harzburgite. Vein samples (δ^7Li = +3.0 to +5.0) do not record a significant slab-derived δ^7Li signature. These observations can be reconciled if slab Li diffusively re-equilibrates in the mantle wedge. Modeling demonstrates that Li equilibration of small (1–2 cm width) veins or melt conduits is achieved at mantle wedge temperatures within 10^1–10^5 years. We conclude that strongly fractionated Li isotopic signatures cannot be sustained for long periods in the sub-arc mantle, at least at shallow (<70 km) depths.

Keywords Lithium · Li isotopes · Sub-arc mantle · Mantle xenoliths · Metasomatism · Kamchatka

Communicated by J. Hoefs.

Electronic supplementary material The online version of this article (doi:10.1007/s00410-009-0378-5) contains supplementary material, which is available to authorized users.

R. Halama · R. L. Rudnick · W. F. McDonough
Department of Geology, University of Maryland, College Park, MD 27042, USA

I. P. Savov
Department of Terrestrial Magnetism, Carnegie Institution of Washington, Washington, DC 20015, USA

R. Halama (✉)
Institut für Geowissenschaften and SFB 574, Universität Kiel, 24098 Kiel, Germany
e-mail: rh@min.uni-kiel.de

I. P. Savov (✉)
School of Earth and Environment, Institute of Geophysics and Tectonics, The University of Leeds, Leeds LS2 9JT, UK
e-mail: i.savov@see.leeds.ac.uk

Introduction

Subduction zones are the most important sites for cycling of elements between the surface and the interior of the Earth. Devolatilization of subducting lithosphere triggers the generation of arc magmas within the mantle wedge, which is enriched in fluid-mobile components derived from the subducted slab. While most inferences on the processes occurring within the mantle wedge derive from studies of arc magmas and peridotite melting experiments, mantle xenoliths from arcs can provide complementary information.

Mantle xenoliths from arcs are relatively scarce compared to those from other tectonic settings (Arai and Ishimaru 2008; Nixon 1987), yet these peridotites provide an opportunity to investigate geochemical processes related to the material transfer from subducted slabs to arc volcanoes, such as depletion of magmatic components and re-fertilization by fluid- or melt–rock interaction. Moreover, arc peridotite xenoliths offer insights on the origin

and geochemical characteristics of metasomatic agents within the sub-arc mantle. Currently, debate surrounds the issue of whether the primary metasomatizing agent in the mantle wedge of arcs is an aqueous fluid or a silicate melt, as the chemical characteristics of arc volcanic rocks could be explained by both mantle–melt interaction (Kelemen et al. 2003; Prouteau et al. 2001) and slab fluid additions to the mantle (Eiler et al. 1998; Elliott 2003).

The Li isotope system has the potential to track recycled material from the Earth's surface or from the fluid-modified sub-arc mantle into the convective upper mantle (Elliott et al. 2004, 2006; Tomascak et al. 2002). Li is a sensitive tracer of fluid flow since it is fluid-mobile (Brenan et al. 1998b) and its two stable isotopes (^{6}Li and ^{7}Li) are significantly fractionated (up to 70‰) at low temperatures due to their large relative mass difference ($\sim$15%). To date, there are few studies of the Li isotopic composition of sub-arc mantle xenoliths (Ionov and Seitz 2008; Nishio et al. 2004). It was initially assumed that the sub-arc mantle might be enriched in ^{7}Li because of the transfer of heavy Li from the subducted altered oceanic crust (AOC) into the mantle wedge (Elliott et al. 2004; Tomascak et al. 2002). Subsequently, it was proposed that the heavy Li isotopic signature of the sub-arc mantle may be sampled in mid-ocean ridge basalts (Elliott et al. 2006) and hence reflect large-scale mantle cycling (Elliott et al. 2004), although the rapid diffusivity of Li (Coogan et al. 2005; Richter et al. 2003) raises some doubts about the efficacy of this process (Halama et al. 2008). Moreover, the isotopic composition of Li transferred from the subducted slab into the mantle wedge is uncertain because of the large natural variation of δ^{7}Li in subducted materials (Bouman et al. 2004; Chan et al. 1992, 2006a) and possible isotopic fractionations during dehydration (Benton et al. 2004; Marschall et al. 2007; Wunder et al. 2006; Zack et al. 2003). Further complexity stems from the effects of diffusion-controlled interactions with Li-bearing fluids, which are able to cause inter-mineral disequilibria in mantle xenoliths and may consequently mask the original Li isotopic signatures of their source regions (Ionov and Seitz 2008; Jeffcoate et al. 2007; Rudnick and Ionov 2007). Hence, the relative influences of late-stage diffusion effects and contributions from slab-derived melts/fluids are still debated.

Kamchatka is among the few arcs on Earth where mantle xenoliths are abundant and thus represents a key locality for assessing the effects of subduction-related metasomatism of the sub-arc mantle (Arai and Ishimaru 2008; Ionov and Seitz 2008; Ishimaru et al. 2007; Kepezhinskas and Defant 1996; Kepezhinskas et al. 1995; Widom et al. 2003). Mantle xenoliths carried in calc-alkaline lavas from Avachinsky volcano comprise highly depleted harzburgites intersected by pyroxenitic veins and record modal and cryptic metasomatism of the host peridotite (Kepezhinskas et al. 1996; Widom et al. 2003).

In this study, we focus on two xenoliths from Avachinsky that contain veins representing modal metasomatism in the sub-arc mantle. Hence, they are well suited for studying the Li elemental and isotopic compositions of slab-derived metasomatic agents and lend constraints on Li isotope cycling in subduction zones. To elucidate the nature of the metasomatic agent, we have combined the Li elemental and isotopic study with a detailed petrographic and trace element investigation of the vein minerals in order to discriminate fluid- versus melt-related metasomatism. We find that mineral and calculated bulk vein compositions show enrichment in several trace elements (U, Sr, Pb) commonly associated with fluid-driven metasomatism. However, harzburgites and the cross-cutting pyroxenite veins are in Li elemental and isotopic equilibrium and the Li isotopic composition of the mantle xenoliths overlaps with those of the host arc lavas. These features are consistent with diffusive equilibration and indicate no post-crystallization Li redistribution associated with the xenolith entrainment in the host lavas. We argue that the veins have inherited specific trace element characteristics from a slab-derived fluid, but represent the crystallization products of a boninitic melt that has equilibrated with the mantle wedge.

Geological setting and samples

The xenoliths are from Avachinsky volcano (53°15′N, 158°51′E), in southern Kamchatka, which is one of the active volcanic centers in the Eastern Volcanic Front of the Kamchatka arc and is situated 200 km NW of the Kuril-Kamchatka trench (Fig. 1). Formation of the Kamchatka convergent margin is related to subduction of the Pacific plate beneath the Eurasian plate at 7–9 cm/year. In the northern segment of the arc, young (<25 Ma) and hot oceanic lithosphere formed in the Komandorsky Basin is subducted, whereas subduction of old (87–104 Ma) lithosphere of the Pacific plate takes place in the central and southern arc segments (Renkin and Sclater 1988). Avachinsky is located $\sim$120 km above the Benioff zone (Gorbatov et al. 1997) and the depth to the Moho is $\sim$37 km (Levin et al. 2002). A layer of low seismic velocities, interpreted as the asthenospheric mantle wedge, has been identified at a depth interval from 70 to 130 km beneath Eastern Kamchatka (Nizkous et al. 2006).

Ultramafic xenoliths of mantle origin have been found at several volcanic centers from the Kamchatka arc (Bryant et al. 2007; Ishimaru et al. 2007; Kepezhinskas and Defant 1996; Kepezhinskas et al. 1995). Based on geochemical data for both mantle xenoliths and arc lavas, it has been

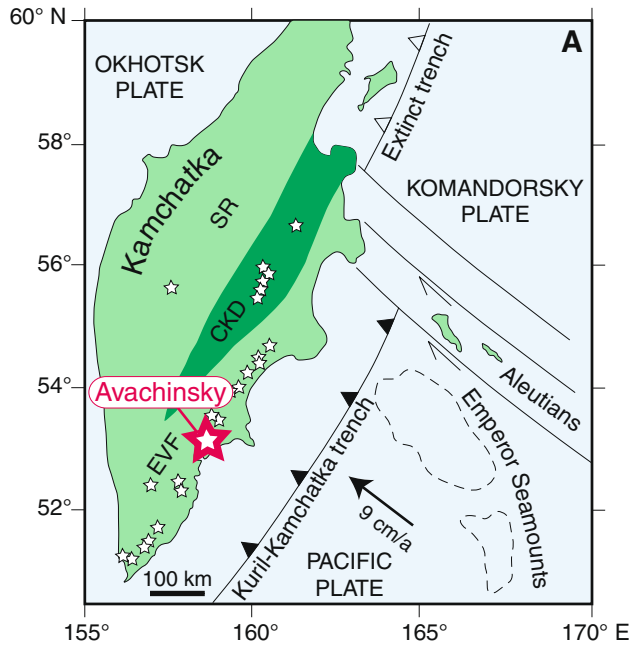

Fig. 1 Simplified map of the Kamchatka peninsula with Quaternary volcanic belts and tectonic structures of the Kamchatka-Aleutian arc junction modified from Portnyagin et al. (2005). *EVF* Eastern Volcanic Front, *SR* Sredinny Range, *CKD* Central Kamchatka Depression

proposed that modifications of the mantle wedge are caused predominantly by the infiltration of fluids in the southern segment of the arc, whereas siliceous melts as well as fluids contribute to wedge metasomatism in the northern segment (Kepezhinskas et al. 1997; Münker et al. 2004). At Avachinsky, where several Holocene (7,200–3,500 years B.P.) pyroclastic units contain ultramafic xenoliths (Braitseva et al. 1998), the eruption products range in composition from picrite to dacite, but are primarily composed of calc-alkaline andesites and basalts. Several detailed petrological and geochemical studies of the Avachinsky mantle xenoliths have been carried out (Arai et al. 2003; Kepezhinskas and Defant 1996, 2001; Kepezhinskas et al. 2002; Widom et al. 2003). Recently, Ishimaru et al. (2007) and Ishimaru and Arai (2008a, b, c) provided a detailed account of metasomatism in the mantle wedge as inferred from Avachinsky xenoliths. Ionov and Seitz (2008) studied the Li isotopic composition of Avachinsky xenoliths, focusing on peridotites without modal and textural heterogeneities and intentionally excluding veined varieties. They concluded that the shallow mantle in the Kamchatka arc has MORB-type Li isotopic signatures and suggested that Li isotopes in xenoliths carried in pyroclastic rocks that cool quickly, like at Avachinsky, are not significantly affected by the Li isotope disequilibria seen in lava-hosted xenoliths that cool more slowly. Since xenoliths can be quite heterogeneous, each sample may provide important geological and geochemical information. In this study, we focus on two spinel-harzburgite xenoliths that contain pyroxenite veins up to 2–3 cm in width (Fig. 2). The harzburgites are similar to samples from Avachinsky described previously (Arai et al. 2003; Ionov and Seitz 2008; Ishimaru et al. 2007; Kepezhinskas et al. 2002). The pyroxenites contain variable amounts of orthopyroxene, clinopyroxene and amphibole (Fig. 2).

Analytical methods

The size of the two veined xenolith samples is ~12 × 3 cm for AVX-60 and ~14 × 6 cm for AVX-61. About 10 g of whole-rock powder were prepared by hand using agate mortar and pestle. For isotopic analyses, samples were dissolved in a 3:1 mixture of concentrated HF–HNO_3 in Savillex screw-top beakers on the hotplate (120°C), and dried residua were repeatedly picked up with concentrated HCl until solutions were clear.

Whole rock major element compositions

Major and trace element concentrations (Table 1) were determined using X-ray fluorescence (XRF) spectrometry on fused glass discs from ~1.5 g whole-rock powder. Measurements were performed at the University of Tübingen on a Bruker AXS S4 Pioneer spectrometer by standard analytical techniques. Calibration curves were determined using 21–32 standards, depending on the element analyzed. Analytical uncertainties are less than 1% for major elements and between 2 and 5% for trace elements (Shang et al. 2007).

Mineral chemistry

Mineral compositions (supplementary material) were determined using electron microprobes at the Geophysical Laboratory of the Carnegie Institution for Science, Washington (Jeol JXA-8800), the University of Maryland, College Park (Jeol JXA-8900), and at the University of Kiel (Jeol JXA-8900R). Operating conditions were 15 kV acceleration voltage, 10 nA emission current and 5 mm spot size. Both natural and synthetic standards were used for calibration. Measuring times on the peak positions were 10 s for Si, Mg and Al, 20 s for Ti, 30 s for Na and Ca, and 60 s for Mn, Cr and Ni.

In situ mineral trace element compositions

In situ determinations of trace element contents in individual minerals were determined using a Thermo Finnigan Element 2 single collector sector field ICP mass

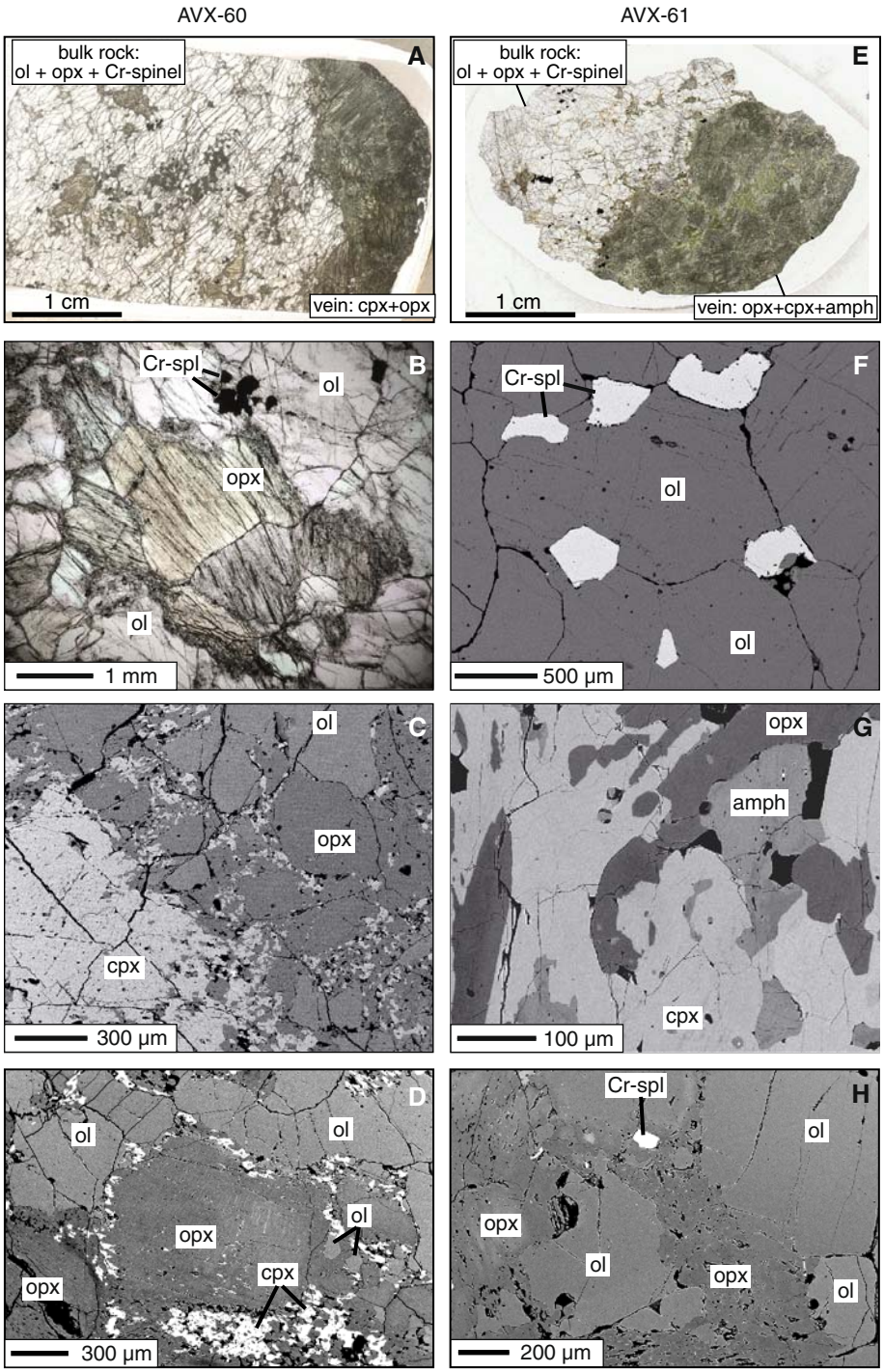

Fig. 2 Photographs and back-scattered electron (BSE) images of Avachinsky mantle xenoliths. **a–d** Sample AVX-60, **e–h** sample AVX-61. **a** Thin section of sample AVX-60 with clinopyroxene (cpx)–orthopyroxene (opx) vein. **b** Microphotograph of fibrous orthopyroxene, olivine (ol) and Cr-spinel (Cr-spl) in harzburgite. **c** BSE image of the contact between vein, comprising cpx and opx, and olivine-dominated harzburgite. **d** BSE image of the harzburgite-vein contact zone with remnants of olivine surrounded by metasomatic opx and enrichments of cpx along grain boundaries between olivine and opx. **e** Thin section of sample AVX-61 with opx–cpx–amphibole (amph) vein. **f** BSE image of coarse-equant texture with olivine and Cr-spinel in harzburgite. **g** BSE image of metasomatic vein with opx, cpx and amphibole. **h** BSE image of harzburgite-vein contact zone with metasomatic opx replacing olivine and opx veinlets intruding into the harzburgite

spectrometer coupled to a New-wave UP-213 nm wavelength laser ablation unit at the University of Maryland. Because of delays produced by the need for a large magnet jump, Li and trace elements with masses >80 (Rb–U) were analyzed separately. For the higher mass trace elements, NIST 610 glass was used for calibration and BCR-2g was analyzed as reference material. ^{43}Ca was used as internal standard to correct for ablation yield differences between and during individual analyses. For Li, BCR-2g was used for calibration, ^{57}Fe was used as internal standard, and NIST 610 glass was analyzed as a reference material. Calculated Li concentrations using ^{57}Fe as internal standard and BCR-2g for calibration were preferred over those using ^{43}Ca and NIST 610 because the former resulted in a better agreement with solution ICP-MS analyses and yielded smaller inter-grain variations. For instance, olivine (orthopyroxene) from sample AVX-61 has 1.65 ± 0.05 (0.99 ± 0.30) ppm Li calculated using ^{57}Fe and BCR-2g

Table 1 XRF whole-rock analyses and Sr isotopic analyses of Avachinsky veined mantle xenoliths and host lavas

Sample #	AVX-33	AVX-45	AVX-49	AVX-60	AVX-61	AVX-60 vein	AVX-61 vein	AVX-35-B	AVX-49-B	AVX-60-B
Rock type	Harzburgite	Harzburgite	Harzburgite	Harzburgite	Harzburgite	Pyroxenite	Pyroxenite	BA	BA	BA
Major elements (wt%)										
SiO_2	42.92	41.39	43.56	42.55	44.40	51.58	55.68	53.51	54.12	54.22
TiO_2	0.02	0.01	0.02	0.01	0.02	0.04	0.05	0.91	0.80	0.89
Al_2O_3	0.53	0.32	0.45	0.45	0.78	1.32	1.98	18.44	20.24	19.73
Cr_2O_3	0.39	0.49	0.55	0.20	0.53	0.45	0.46	0.01	0.00	0.01
Fe_2O_3	8.93	9.23	8.72	9.49	8.76	5.02	6.12	8.44	7.03	7.25
NiO	0.31	0.31	0.29	0.30	0.27	0.09	0.06	0.01	0.00	0.01
MnO	0.13	0.13	0.13	0.14	0.13	0.12	0.14	0.16	0.12	0.14
MgO	46.20	47.08	44.93	45.12	44.64	25.82	33.11	5.06	3.53	3.67
CaO	0.60	0.62	0.72	0.68	0.52	14.13	1.33	9.03	9.18	8.85
Na_2O	0.00	0.00	0.00	0.00	0.00	0.11	0.00	3.43	3.62	3.76
K_2O	0.00	0.00	0.00	0.00	0.00	0.00	0.00	0.49	0.61	0.56
P_2O_5	0.01	0.00	0.01	0.01	0.02	0.02	0.02	0.15	0.15	0.17
LOI	−0.23	−0.11	−0.29	−0.15	−0.34	0.42	0.05	−0.12	0.24	0.36
Total	99.81	99.47	99.09	98.81	99.72	99.12	99.00	99.50	99.65	99.62
Trace elements (ppm)										
Ba	ND	17.9	ND	ND	ND	ND	41.4	207	337	363
Co	119	122	113	118	112	48.4	56.7	49.3	36.2	34.0
Cr	2,692	3,355	3,780	1,399	3,606	3,080	3,152	56.4	32.1	87.8
Ni	2,426	2,460	2,290	2,360	2,122	741	456	63.7	16.7	63.6
Rb	4.0	ND	ND	ND	ND	ND	7.3	8.0	11.6	9.6
Sr	ND	ND	ND	ND	ND	4.5	ND	310	411	348
V	33.2	30.6	42.8	27.2	30.3	132	59.6	230	228	209
Y	ND	ND	ND	ND	ND	ND	ND	25.3	14.5	24.5
Zn	28.9	39.8	37.4	32.3	29.5	ND	ND	61.2	44.0	47.6
Zr	ND	ND	ND	ND	ND	8.1	5.2	90.0	78.6	98.6
Ce	ND	ND	ND	ND	ND	ND	ND	ND	ND	ND
Eu	0.3	0.3	0.3	0.4	0.3	0.2	0.3	1.1	1.3	0.9
Nd	ND	ND	ND	ND	ND	3.8	12.2	14.4	6.0	25.8
Yb	0.2	0.6	0.4	0.3	0.1	0.2	0.5	2.2	1.6	2.3
$^{87}Sr/^{86}Sr$	0.705896[a]	0.70356		0.708624	0.706687	0.703988	0.704810			

BA basaltic andesite, *ND* not detected

[a] Analysis of separated orthopyroxene

and 2.31 ± 0.46 (0.81 ± 0.61) ppm Li calculated using ^{43}Ca and NIST 610, compared to 1.6 (1.2) ppm Li based on the solution analysis.

Trace element concentrations determined for reference materials are given in Tables 2 and 3. The laser beam diameter on the sample surface was 40 μm for calibration standards and 80–100 μm for samples. Spot analyses were applied with a laser repetition rate of 8–12 Hz and an output power of ~2 J/cm^2. Total acquisition time was 80 s per analysis, allowing about 20 s for background followed by 60 s for laser ablation. The detection limit was defined as three standard deviations above background level, which equates to a 95% confidence that the measured signal is significantly above background. For a 80 μm spot size, the detection limits are approximately 0.1 ppm for Rb, 0.2 ppm for Sr, 0.01 ppm for Cs and Ba, 0.005 ppm for Pb and 0.004 ppm for all other trace elements.

Sr isotopes

Strontium was extracted from unspiked dissolved rock by conventional ion-exchange chromatographic techniques in the clean laboratories of the Department of Terrestrial

Table 2 Trace element concentrations of vein minerals from Avachinsky mantle xenoliths, calculated bulk vein compositions and reference material analyses

	In situ mineral analyses				Calculated bulk veins		Reference material analyses			GeoReM
Sample	AVX-60 vein	AVX-61 vein	AVX-60 vein	AVX-60 vein	AVX-60 vein	AVX-61 vein	BCR-2g			BCR-2g
Rock type	Pyroxenite	Pyroxenite	Pyroxenite	Pyroxenite	Pyroxenite	Pyroxenite	Basalt			Basalt
Mineral	Cpx	Amph	Opx	Opx			Glass			Glass
Number of analyses	11	7	3	REE calculated[a]			15			Preferred values
Modal proportions opx/cpx/amph					0.3/0.7/0.0	0.80/0.15/0.05	Average	SD (1σ)	RSD (in %)	
Trace elements (in ppm)[b]										
Li[c]	1.08	0.96	1.31		1.15	1.26				
Ti	135	589	70.7		116	106	12,950	300	2.3	13,605
Rb	0.124	7.99	ND		0.087	0.418	47.7	2.3	4.8	47.0
Sr	7.23	51.39	0.071		5.08	3.71	329	17	5.2	342
Y	0.826	2.52	0.085		0.604	0.318	30.9	1.7	5.5	35.0
Zr	0.591	16.41	0.075		0.436	0.969	170	9	5.3	184
Nb	0.005	0.534	ND		0.003	0.027	10.4	0.6	5.8	12.5
Ba	0.746	112.1	0.131		0.562	5.82	646	34	5.3	683
La	0.062	1.01	0.002	0.0003	0.043	0.060	25.7	1.5	5.8	24.7
Ce	0.148	1.65	0.005	0.0011	0.104	0.106	52.4	3.1	5.9	53.3
Pr	0.025	0.179	0.001	0.0003	0.017	0.013	6.44	0.47	7.3	6.70
Nd	0.132	0.763	0.005	0.0022	0.093	0.060	28.7	2.1	7.3	28.9
Sm	0.053	0.191	0.001	0.0018	0.038	0.019	6.59	0.56	8.5	6.59
Eu	0.020	0.085	0.003	0.0009	0.014	0.008	2.02	0.15	7.4	1.97
Gd	0.077	0.238	ND	0.0045	0.055	0.027	5.98	0.36	6.0	6.71
Tb	0.016	0.044	0.003	0.0013	0.012	0.006	1.00	0.08	8.0	1.02
Dy	0.124	0.355	ND	0.0126	0.091	0.046	6.11	0.57	9.3	6.44
Ho	0.033	0.091	0.004	0.0043	0.024	0.013	1.24	0.09	7.3	1.27
Er	0.102	0.319	0.017	0.0163	0.076	0.044	3.43	0.31	9.0	3.70
Tm	0.016	0.050	ND	0.0032	0.012	0.008	0.46	0.03	6.5	0.51
Yb	0.137	0.460	ND	0.0320	0.106	0.069	3.29	0.29	8.8	3.39
Lu	0.023	0.087	0.008	0.0062	0.018	0.013	0.49	0.04	8.2	0.50
Hf	0.021	0.495	0.002		0.015	0.029	4.69	0.20	4.3	4.84
Ta	0.001	0.047	ND		0.000	0.002	0.61	0.04	6.6	0.78
Pb	0.047	0.586	ND		0.033	0.036	11.0	0.82	7.5	11.0
Th	0.004	0.085	ND		0.003	0.005	5.93	0.41	6.9	5.90
U	0.003	0.065	ND		0.002	0.004	1.79	0.14	7.8	1.69

[a] REE concentrations in orthopyroxene were calculated based on opx/cpx partition coefficients after Lee et al. (2007)

[b] Trace element concentrations were determined by laser ICP-MS using NIST-610 glass as reference material and Ca as internal standard element

[c] Li concentrations were calculated using BCR-2g as reference material with Fe as internal standard element

Table 3 Li concentrations and Li isotopic compositions of Avachinsky mantle xenoliths and host lavas

Sample	Material	δ^7Li	Li (ppm)	
			Solution	Laser
Harzburgites				
AVX 33	Ol	4.1	1.7	
	Ol repl.	2.8	2.1	
	Ol avg.	3.5	1.9	
	Opx	5.2	1.2	
	Opx repl.	4.8	1.3	
	Opx avg.	5.0	1.2	
AVX 35	Ol	4.7	1.3	
AVX 45	Ol	3.0	1.5	
	Opx	5.3	1.0	
AVX 49	Ol	4.3	1.6	
	Opx	4.4	0.9	
AVX 60	Ol	5.6	1.9	1.39–2.33
	Opx	–	–	0.73–1.30
AVX 61	Ol	4.8	1.6	1.57–1.68
	Ol repl.	5.6	2.1	
	Ol avg.	5.2	1.9	
	Opx	4.2	1.2	0.71–1.44
Pyroxenite veins				
AVX 60v	Bulk vein	5.0	0.8	
	Cpx	3.0	1.3	0.63–1.38
AVX 61v	Bulk vein	3.5	2.0	
	Amphibole	–	–	0.92–1.00
	Opx	3.8	1.5	1.23–1.42
	Opx repl.	3.9	1.3	1.23–1.42
	Opx avg.	3.9	1.4	
Basaltic andesite lavas				
AVX 35-B	Whole-rock	4.9	8.0	
AVX 49-B	Whole-rock	5.1	10.5	
AVX 60-B	Whole-rock	3.5	11.0	
Reference materials				
JB-2	Whole-rock	4.7 ± 1.3 (2σ, $n = 5$)	8.0 ± 0.7 (1σ, $n = 3$)	
BHVO-1	Whole-rock	4.7 ± 1.2 (2σ, $n = 6$)	4.6 ± 0.3 (1σ, $n = 3$)	
UMD-1	Solution	55.8 ± 1.0 (2σ, $n = 30$)		
IRMM-016	Solution	0.3 ± 0.7 (2σ, $n = 30$)		
NIST 610	Glass			500 ± 32 (1σ, $n = 16$)

Ol olivine, *Opx* orthopyroxene, *Cpx* clinopyroxene, *Repl.* replicate dissolution, *avg.* average composition

Magnetism of the Carnegie Institution. Measurements were made by thermal-ionization mass spectrometry (TIMS) on a Thermo Finnigan Triton multicollector mass spectrometer running in static mode. $^{87}Sr/^{86}Sr$ ratios were normalized for mass fractionation to $^{86}Sr/^{88}Sr = 0.1194$. The instrumental error of the $^{87}Sr/^{86}Sr$ ratios, reported as standard error (2σ of the mean of 190 single determinations), is 0.000005. The average $^{87}Sr/^{86}Sr$ obtained from replicate measurements of NIST SRM-987 was 0.710246 ± 0.000024 (2σ, $n = 3$). The total blanks for Sr were negligible for the samples during the period of measurement.

Lithium isotopes

Li concentrations and Li isotopic compositions of mineral separates and bulk veins were determined following acid digestion and column chemistry methods described previously in Rudnick et al. (2004). Measurements were carried

out using a Nu Plasma MC-ICP-MS employing the analytical protocol of the University of Maryland (Teng et al. 2004). Each sample analysis is bracketed before and after by measurement of the L-SVEC standard. The δ^7Li value of the sample ($\delta^7\text{Li} = (^7\text{Li}/^6\text{Li}_{\text{sample}}/^7\text{Li}/^6\text{Li}_{\text{standard}}) - 1) \times 1{,}000$) is calculated relative to the average of these two bracketing L-SVEC runs. Analytical uncertainty of this method is ±1‰ (2σ) based on long-term replication of an in-house standard, UMD-1 (a purified Li solution from Alfa Aesar®), and the international SRM IRMM-016 (Qi et al. 1997). Both standard solutions were analyzed two to three times during the course of each analytical session. Results for the pure Li standard solutions as well as results for international reference materials (JB-2 and BHVO-1) are presented in Table 3. The values obtained agree well with previously published data [JB-2: +4.2 to +6.8 (Jeffcoate et al. 2004; Magna et al. 2004; Marks et al. 2007); BHVO-1: +4.3 to +5.8 (Bouman et al. 2004; Chan and Frey 2003; Halama et al. 2007; James and Palmer 2000; Rudnick et al. 2004)]. Li concentrations were determined by comparing signal intensities of sample solutions with a 50 ppb L-SVEC solution and then adjusting for sample weight. The accuracy of this method was established before (Teng et al. 2004), and the precision is better than ±10% at the 2σ level (Teng et al. 2006).

Petrology of veined mantle xenoliths

Since our samples are similar to previously studied mantle xenoliths from Avachinsky (Arai et al. 2003; Ionov and Seitz 2008; Ishimaru et al. 2007; Kepezhinskas et al. 2002), petrologic and geothermometry data are only briefly described. Representative mineral analyses are provided in the supplementary material. The Avachinsky xenoliths are refractory spinel-harzburgites dissected by pyroxenite veins. The harzburgites contain olivine ($Fo_{90–92}$), orthopyroxene ($En_{90–95}$) and spinel (Cr# = 64–71). NiO contents in olivine vary from 0.3 to 0.5 wt%, which is typical for upper mantle olivine (e.g., Kelemen et al. 1998), but lower than abnormally Ni-rich olivines formed by interaction with sulfide melts (Ishimaru and Arai 2008a). Both NiO concentrations and Mg# do not show systematic zoning within olivines, and the intra-grain variation for Mg# is below 0.01 units. Several olivine grains are characterized by a rimward increase in CaO with an enrichment factor of ~3 to 4 and a mean difference of 0.034 wt% CaO ($n = 4$). Similar rim enrichments in CaO in olivine from other peridotite xenoliths were interpreted to reflect either heating of the mantle during magmatic activity or heating associated with entrainment and transport of xenoliths in the host basalts (Luhr and Aranda-Gómez 1997; Zipfel and Wörner 1992). Most orthopyroxenes in the harzburgite occur in radial aggregates and appear to form at the expense of olivine. There is some inter-grain variability in Mg# for orthopyroxene, but most have Mg numbers around 0.91–0.92. On average, Mg# in orthopyroxene is slightly higher than in olivine, which is typical for equilibrated peridotites and similar to Avachinsky xenoliths that have been investigated previously (Ishimaru and Arai 2008b). Orthopyroxene Mg# as high as 0.97 as reported for highly metasomatized Avachinsky xenoliths (Ishimaru and Arai 2008b) have not been observed in our harzburgite samples, although a few have Mg# up to 0.95. Spinels are unzoned with little inter-grain chemical variability.

The very low modal clinopyroxene content (<0.5%), the refractory mineral chemistry (high Cr# of spinels, high Mg# of olivines and orthopyroxenes), and the low bulk rock Al_2O_3 and CaO concentrations (0.3–1.2 and 0.5–0.7 wt%, respectively) are evidence for significant melt extraction. Equilibration temperatures of the harzburgites are 880–1,090°C based on the Ca-in-orthopyroxene thermometer of Brey and Köhler (1990). A somewhat higher temperature range of 950–1,120°C was calculated using the olivine-spinel Mg–Fe exchange thermometer (Ballhaus et al. 1991). Maximum pressures of 3.4–3.8 GPa were estimated based on the stability of Cr-spinel (O'Neill 1981). These thermobarometric results agree well with previously published data on Avachinsky mantle xenoliths (Ishimaru et al. 2007; Kepezhinskas et al. 2002).

The pyroxenite veins are olivine-free websterites and comprise orthopyroxene ($En_{88–94}$) and clinopyroxene ($En_{54–48}Wo_{43–49}$). Minor amphibole (~5%) occurs only in the vein from sample AVX-61 (abbreviated as AVX-61v). The amphibole is magnesio-hornblende with 9.4–10.8 wt% Al_2O_3, $(Na + K)_A = 0.5–0.6$, Mg# = 0.92–0.95 and high Cr_2O_3 concentration (1.3–2.5 wt%). Vein orthopyroxene compositions overlap with those of orthopyroxenes from the harzburgitic host. There is no systematic zoning in Mg# and intra-grain variations are relatively small compared to inter-grain chemical variability. In sample AVX-60, a 100–300 μm wide band of orthopyroxene has formed at the contact of vein clinopyroxene with olivine (Fig. 3). From the olivine side toward the clinopyroxene side, Al_2O_3 contents decrease whereas Cr_2O_3 contents increase. This behavior in orthopyroxene is unlike the commonly found positive correlations between these two oxides (e.g., Heinrich and Besch 1992) and suggests a reaction relationship. Like for vein orthopyroxene, vein clinopyroxene intra-grain chemical variations are minor compared to variations from grain to grain. Mg# of clinopyroxene ranges from 0.92 to 0.98, within the range reported in previous studies (Ishimaru et al. 2007, Ishimaru and Arai 2008b). Temperature estimates for the veins, based on two-pyroxene thermometry (Brey and Köhler 1990), range from 730 to 1,050°C, with 90% falling between 750 and 920°C. The

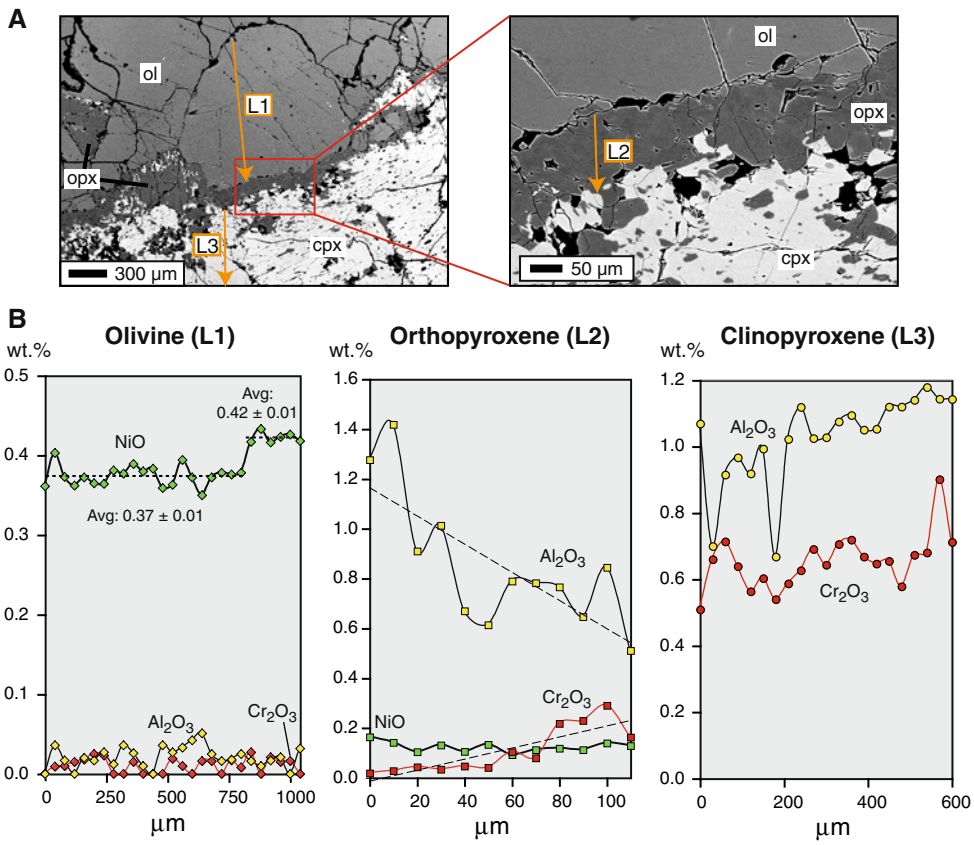

Fig. 3 **a** BSE images of the contact zone between the harzburgite (*upper part*) and pyroxenite vein (*lower part*) in sample AVX-60. Note the band of orthopyroxene at the contact between olivine and clinopyroxene. The *orange arrows* indicate the location of the profiles measured by microprobe shown in **b**. Note the increase in NiO content in olivine toward the contact with opx, where *stippled lines* denote average concentrations. In opx, gradients of Al_2O_3 and Cr_2O_3 are directly opposed and *dashed lines* are best-fit linear regressions

overall temperature range of Ca-in-orthopyroxene thermometry for vein orthopyroxenes (760–1,160°C) overlaps the range determined by two-pyroxene thermometry, but yields a slightly higher average (924 ± 120°C; $n = 22$). Thus, there is no obvious temperature difference between veins and surrounding harzburgites.

Contacts between harzburgite and veins are irregular with a gradational transition (Fig. 2). Small (mostly <100 µm) olivine grains, which are partly or completely surrounded by orthopyroxene, occur in the outermost parts of the veins. These olivines appear to be remnants that have not been fully replaced by the orthopyroxene. This interpretation is supported by the presence of orthopyroxene veinlets intruding into the harzburgitic host rock. A reaction relationship between veins and harzburgite is also indicated by the concentration of clinopyroxene at grain boundaries between olivine and vein orthopyroxene (Fig. 2) and by the formation of a 100–300 µm thick band of orthopyroxene at the contact between olivine and vein clinopyroxene (Fig. 3). All these features suggest a metasomatic origin of the pyroxenite veins.

The temperatures calculated for both harzburgites and pyroxenites can be used to evaluate the depth of origin of the xenoliths. Assuming a geothermal gradient of 22.5°C/km in the crust, a crustal thickness of 35 km, and a gradient of 10°C/km beneath the Moho (Manea and Manea 2007), temperatures of ~1,140°C would be reached at 70 km depth. Hence, it appears likely that the two xenoliths investigated here may be derived from depths <70 km, i.e., from within the mantle lithosphere.

Results

Trace element composition of vein minerals and bulk veins

Pyroxenes

Vein clinopyroxene from sample AVX-60v is depleted in trace elements relative to the primitive mantle, but has relative enrichments in U, Pb, Sr and Li and a negative Nb–Ta anomaly (Fig. 4a). The rare earth element (REE) pattern is smooth, with a depletion of LREE relative to HREE ($(La/Yb)_N = 0.31$). Compared to clinopyroxenes in mantle xenoliths from intraplate settings (squares and diamonds in Fig. 4a), the vein clinopyroxene from Avachinsky is distinct in its much lower trace element concentrations (up to 2 orders of magnitude) and the absence of negative Ba, Pb, Ti and Li spikes. Clinopyroxene from sample AVX-61v

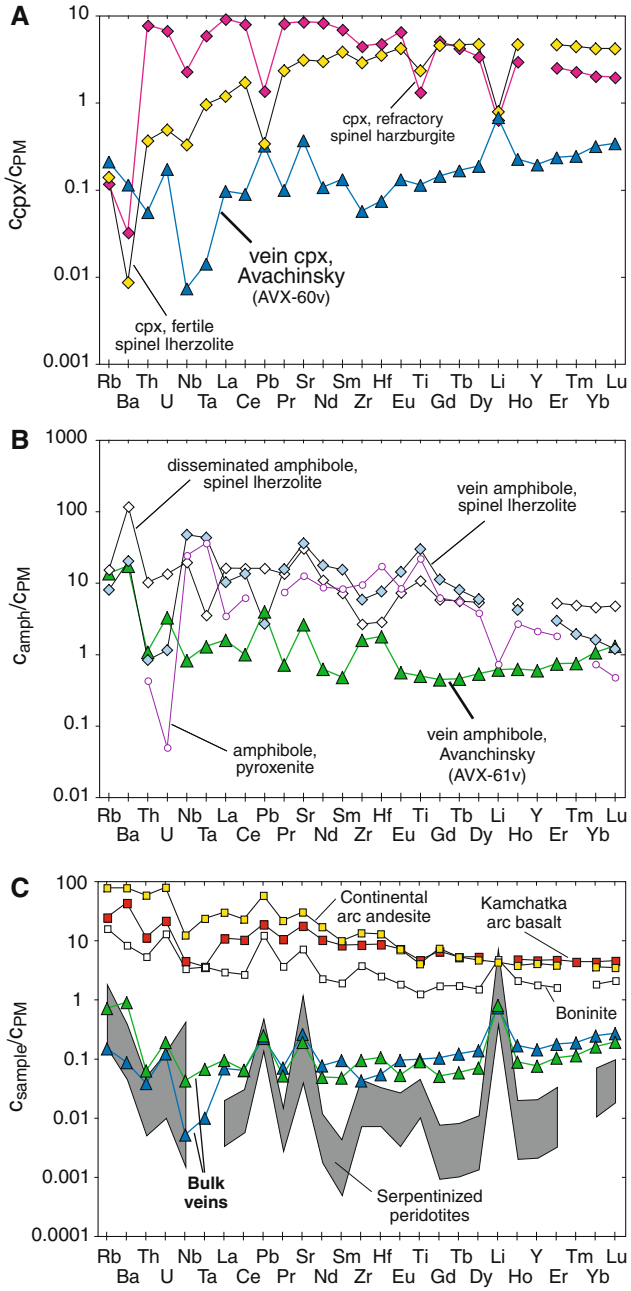

Fig. 4 Primitive mantle-normalized trace element diagrams of **a** clinopyroxene (sample AVX-60), **b** amphibole (sample AVX-61) and **c** calculated bulk vein compositions from metasomatic veins in Avachinsky mantle xenoliths. For comparison, clinopyroxenes from a refractory spinel harzburgite and from a fertile spinel lherzolite, both xenoliths in basanitic lavas (Eggins et al. 1998) are displayed in **a**. In **b**, disseminated and vein amphibole from mantle xenoliths in alkali basalts (Ionov and Hofmann 1995) and an amphibole from a pyroxenite in oceanic crust (Glaser et al. 1999) are shown. The bulk vein compositions (*blue triangles* AVX-60, *green triangles* AVX-61) in **c** were calculated based on modal mineralogy and in situ trace element data (Table 2). They are compared to serpentinized fore-arc peridotites (Savov et al. 2005) and various arc lavas (Kelemen et al. 2003). Primitive mantle values are from McDonough and Sun (1995)

was not analyzed for trace elements due to intergrowth with orthopyroxene and amphibole (Fig. 2) and its relatively small grain size.

Vein orthopyroxene from sample AVX-61v has very low incompatible trace element concentrations, with generally less than 1 ppm for all analyzed elements except for Ti (71 ppm) and Li (1.3 ppm). Since some of the REE are below the detection limit, REE concentrations in orthopyroxene were calculated based on orthopyroxene/clinopyroxene partition coefficients after Lee et al. (2007). Orthopyroxene is characterized by a pronounced depletion of LREE relative to HREE.

Amphiboles

The vein amphibole from sample AVX-61v is enriched in trace elements relative to clinopyroxene, but still depleted relative to the primitive mantle in Ti, Li and most of the REE. Its mantle-normalized trace element pattern shows peaks for U, Pb and Sr, similar to those of clinopyroxene (Fig. 4b). In contrast to clinopyroxene, Zr and Hf are enriched relative to the neighboring REE, but Nb and Ta are not. Also, lithium is not enriched relative to the HREE. The REE pattern of the amphibole is smooth and slightly convex (U-shaped) with $(La/Yb)_N = 1.5$. Like the clinopyroxene, the amphibole has relatively low incompatible trace element contents compared to amphiboles in mantle xenoliths from intraplate settings (Ionov and Hofmann 1995). Although the latter can be somewhat heterogeneous, a few similarities between the sub-arc and intraplate amphiboles, such as positive Ba and Sr peaks, are observed. Differences include positive Ti, negative Li spikes and the absence of positive Pb spikes in the amphiboles from the intraplate settings.

Bulk veins

Bulk vein compositions were calculated based on modal mineralogy and in situ trace element data (Table 2). Modal mineral proportions were constrained from petrographic observations and back-scattered electron images. The degree to which the calculated bulk vein compositions are affected by variations in modal mineralogy was determined by varying mineral proportions by up to 60%, which does not change key features of the trace element patterns. If vein mineral trace element concentrations were not available for a particular sample (e.g., cpx in AVX-61), the mineral composition from the other vein was used in the calculations. By calculating bulk vein compositions, trace elements stored in grain-boundary phases (Hiraga et al. 2004) are not considered. This is an advantage over the use of whole-rock

data since incompatible trace elements can be remobilized by secondary processes and whole-rock element ratios may be disturbed by later events (Condie et al. 2004). Moreover, many of the trace elements discussed here (Li, Sr, REE, Th, Pb) have ionic radii that are small enough that they will not be affected by equilibrium grain-boundary segregation in pyroxene aggregates (Hiraga et al. 2004), so that the analyzed phases are not likely to have lost many trace elements to the grain boundaries by this process.

Trace element contents of the bulk veins are depleted relative to the primitive mantle (Fig. 4c). The two calculated bulk vein compositions show similar mantle-normalized trace element patterns, with a slight increase from the LREE to the HREE ($(La/Yb)_N = 0.28–0.59$) and positive peaks for U, Pb, Sr and Li (Fig. 4c). Differences between the two veins occur only for those elements that are highly enriched in amphibole compared to clinopyroxene (Rb–Ba, Nb–Ta, Zr–Hf), resulting from the differences in the modal abundance of amphibole (0% in sample AVX-60v vs. 5% in sample AVX-61v). However, these minor differences do not affect the general trace element patterns.

The calculated bulk vein compositions mimic several trace element characteristics considered typical for arc volcanic rocks (Kelemen et al. 2003) and serpentinized fore-arc peridotites that were metasomatized by slab fluids (Savov et al. 2005, 2007). Most characteristic are the relative enrichments of Ba and U over Th, Pb over Ce and Sr over Nd (Fig. 4c). The enrichments of Pb and Sr are more pronounced for the serpentinized peridotites than for bulk veins or arc volcanic rocks. For Li, the distinct peak on the primitive mantle-normalized plot for serpentinized peridotites spans three orders of magnitude. There is a smaller, but still pronounced Li enrichment in the bulk veins as well as in the average boninite, but there is no Li enrichment in the Kamchatka arc basalt.

Lithium elemental and isotopic equilibrium

Lithium concentrations in olivine (1.4–2.3 ppm), orthopyroxene (0.7–1.5 ppm), clinopyroxene (0.6–1.4 ppm) and amphibole (0.9–1.0 ppm) are in the range typical for equilibrated minerals in mantle peridotite xenoliths (Fig. 5a) and overlap with results from vein-free Avachinsky xenoliths analyzed by Ionov and Seitz (2008) (olivine: 0.9–1.8 ppm Li, opx: 0.5–1.1 ppm Li). Li concentration data from solution MC-ICP-MS and laser ICP-MS give results that are within analytical uncertainty (Table 3). Li variations from grain to grain in a single sample are small and of a similar order of magnitude to those seen in the study of Ionov and Seitz (2008).

Experimental and empirical Li partitioning data can be used to evaluate equilibrium Li partitioning between coexisting mantle phases (Brenan et al. 1998a; Eggins et al. 1998; Seitz and Woodland 2000). The Li distribution coefficient between olivine and orthopyroxene ($^{Li}D_{ol\text{-}opx}$) for the harzburgites is 1.7 ± 0.1, consistent with Li elemental equilibrium (Eggins et al. 1998; Ottolini et al. 2004; Seitz and Woodland 2000). The distribution of Li between olivine and pyroxenes from the vein is given by $^{Li}D_{ol\text{-}opx(V)} \sim 1.3$ and $^{Li}D_{ol\text{-}cpx(V)} \sim 1.6$, indicating a preference for olivine (Fig. 5b). Such values agree well with those proposed for equilibrium partitioning in the mantle (Eggins et al. 1998; Seitz and Woodland 2000).

Olivines and orthopyroxenes from the harzburgites have δ^7Li values that range from +2.8 to +5.6 (Fig. 6a). The average δ^7Li values of olivines ($\delta^7Li = +4.4 \pm 1.0$; $n = 6$) and orthopyroxenes ($\delta^7Li = +4.7 \pm 0.5$; $n = 4$) are identical to estimates of the upper mantle ($\delta^7Li \sim +4 \pm 2$), based on the isotopic compositions of equilibrated mantle peridotites (Jeffcoate et al. 2007; Magna et al. 2006; Seitz et al. 2004), oceanic basalts (Elliott et al. 2004; Ryan and Kyle 2004; Tomascak et al. 2008) and carbonatites (Halama et al. 2008). $\Delta^7Li_{ol\text{-}opx}$ ($=\delta^7Li_{ol}–\delta^7Li_{opx}$) for the individual samples varies from −2.3 to +1.0 with an average of -0.7 ± 1.5 ($n = 4$). These fractionations are very small and generally overlap within analytical uncertainty (±1‰). They are also very similar to the $\delta^7Li_{ol\text{-}opx}$ values reported by Ionov and Seitz (2008) for other Avachinsky xenoliths [−0.4 to +1.3 with an average of -0.3 ± 0.8 ($n = 6$)]. Experimental data for Li isotope fractionation at mantle temperatures between mantle phases are not available, but empirical studies suggest values from −5 to +4 (Jeffcoate et al. 2007; Magna et al. 2006; Seitz et al. 2006). Here, we follow Rudnick and Ionov (2007) and assume that equilibrium $\delta^7Li_{ol\text{-}opx}$ is zero or at least close to zero, given the absence of measurable Li isotopic fractionation at high (>500°C) magmatic temperatures (Halama et al. 2007; Tomascak et al. 1999). Hence, olivine and orthopyroxene in the harzburgites are isotopically equilibrated.

The δ^7Li of pyroxenes from the veins ($\delta^7Li = +3.0$ to +3.9) and the bulk veins ($\delta^7Li = +3.5$ to +5.0) overlap with that of the surrounding harzburgites (Fig. 6b). The average δ^7Li value of all vein analyses (bulk veins and mineral separates) is $+3.8 \pm 0.8$ ($n = 4$). The isotopic fractionation between olivine in the harzburgite and bulk vein, $\Delta^7Li_{ol\text{-}bulk\ vein}$, is +0.6‰ (AVX 60) and +1.7‰ (AVX 61), hence δ^7Li values overlap within analytical uncertainty. For sample AVX 60, $\Delta^7Li_{ol\text{-}cpx(v)}$ is +2.6‰. Our data suggest isotopic equilibration was achieved between the mantle and the metasomatic veins.

Basaltic andesite host rocks ($\delta^7Li = +3.5$ to +5.1) have the same Li isotopic composition as the mantle xenoliths they carry. These values are typical for mantle-derived rocks. Li concentrations in the host rocks range from 8 to

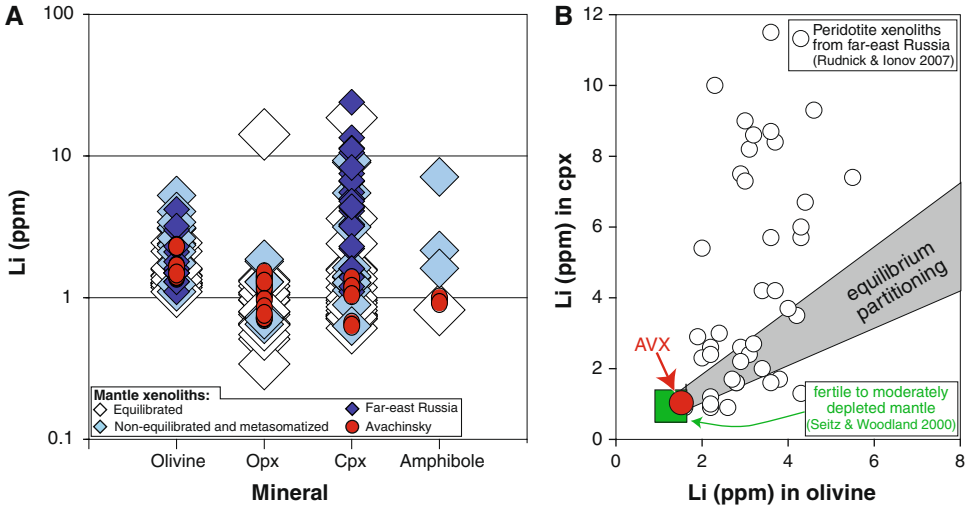

Fig. 5 **a** Li concentrations in minerals from Avachinsky mantle xenoliths compared to minerals from mantle xenoliths from different localities. Equilibrated, non-equilibrated and metasomatized samples are according to the classification and data from Seitz and Woodland (2000). The metasomatized samples from far-east Russia include data from Nishio et al. (2004) and Rudnick and Ionov (2007). **b** Li partitioning between clinopyroxene and olivine in the mantle. The fields for fertile to moderately depleted mantle and for equilibrium partitioning are after Seitz and Woodland (2000). Note that in the Avachinsky xenoliths, clinopyroxene from the metasomatic vein is in equilibrium with olivine from the harzburgite. Data from metasomatized peridotites from far-east Russia (Rudnick and Ionov 2007) are shown for comparison

11 ppm, which is within the range for global arc lavas (Ryan and Langmuir 1987).

Sr isotopes

Strontium isotope compositions of the two harzburgite xenoliths range from 0.7067 to 0.7086 (Table 1). A whole-rock analysis of harzburgite AVX-45 gave $^{87}Sr/^{86}Sr = 0.7036$, whereas an orthopyroxene separate from a different harzburgite xenolith (AVX-33) yielded $^{87}Sr/^{86}Sr = 0.7059$. The two metasomatic veins (samples AVX-60v and AVX-61v) have relatively unradiogenic Sr isotope compositions (0.7040 and 0.7048). All of these values fall within the range observed for off-craton peridotite xenoliths ($^{87}Sr/^{86}Sr \sim 0.701$–$0.710$) (Pearson et al. 2003). They are more radiogenic than the present-day depleted mantle ($^{87}Sr/^{86}Sr = 0.7025$) (Rehkämper and Hofmann 1997) and Pacific MORB ($^{87}Sr/^{86}Sr = 0.7022$–0.7036) (Hofmann 2003). The $^{87}Sr/^{86}Sr$ ratios of the veins fall in the range defined by fluids derived from AOC, with $^{87}Sr/^{86}Sr$ ranging from 0.704 for the Aleutian arc (Singer et al. 2007) to 0.709 for the SE Indian Ridge (Hart et al. 1999). They also overlap with sediment-derived fluids/melts ($^{87}Sr/^{86}Sr = 0.7063$), as modeled for the Aleutian arc (Singer et al. 2007), and serpentinized peridotites from the Mariana fore-arc (0.7047–0.7055), which are interpreted to reflect slab fluid-induced metasomatism (Savov et al. 2007). Vein as well as harzburgite Sr isotope compositions overlap those reported from other Avachinsky xenoliths ($^{87}Sr/^{86}Sr \sim 0.7034$ and ~ 0.7075) (Widom et al. 2003), which were attributed to small additions (<1%) of slab fluids. Hence, inheritance of radiogenic Sr due to slab fluid metasomatism is a viable explanation of our Sr isotope data.

Discussion

Vein crystallization in the sub-arc mantle

In order to relate the trace element patterns of the veins to their origin, we will first evaluate whether they crystallized from a melt or a fluid and then test whether we can detect a signature from a slab-derived metasomatic agent, which may have been inherited by the veins.

High Cr (3,080 and 3,152 ppm for AVX-60v and AVX-61v, respectively) and Ni (741 and 456 ppm) contents in the bulk veins are evidence for crystallization from a mafic melt. Both elements are highly compatible in a variety of minerals coexisting with aqueous fluids at high pressures in the slab, including clinopyroxene, garnet, phengite and lawsonite (Green and Adam 2003), and hence it is unlikely that the veins precipitated from slab-derived aqueous fluids alone. The enrichment of NiO in harzburgite olivine toward the contact with the pyroxenite vein (Fig. 3) supports formation of the vein by melt–rock reaction. The reaction between olivine and SiO_2-rich melt to form orthopyroxene, $2(Mg, Fe, Ni)_2SiO_4 + SiO_2 \rightarrow 2(Mg, Fe)SiO_3 + Ni_2SiO_4$, enhances the NiO content of the remaining olivine in peridotite (e.g., Ishimaru and Arai 2008a) and

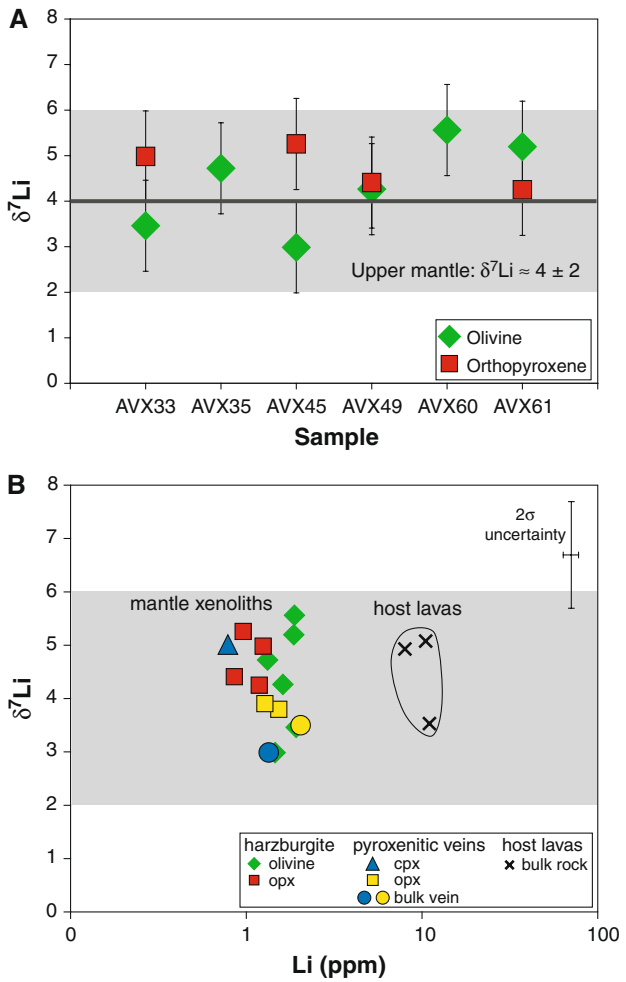

Fig. 6 **a** Li isotopic equilibrium between olivine and orthopyroxene in harzburgite xenoliths from Avachinsky. All isotopic values fall into the range typical for the upper mantle ($\sim 4 \pm 2$), represented by the *gray* field. **b** Li isotopic equilibrium between harzburgite xenoliths, metasomatic veins and host lavas from Avachinsky. Typical δ^7Li values of the upper mantle are indicated by the *gray* field

NiO-rich olivine is left after formation of secondary orthopyroxene (Kelemen et al. 1998).

Given that the veins formed from melts, their trace element compositions are likely influenced by igneous processes (fractional crystallization and crystal accumulation), sub-solidus re-equilibration and/or the composition of the melt from which they crystallized. We will examine each of these factors, in turn.

Fractional crystallization in mantle-derived melts results in increases in incompatible elements, coupled with decreases in compatible elements. The high Cr and Ni concentrations indicate that the veins crystallized from primary mantle melts because both elements are compatible and decrease rapidly in concentration during crystallization (Müntener et al. 2001). The low concentrations of incompatible elements indicate that little evolved intercumulus liquid was incorporated into the vein. Moreover, trends of Fe-enrichment that are usually observed in cumulate pyroxenes from ultramafic complexes (Dick and Bullen 1984; Ozawa 1994; Wilson 1982) do not occur in the vein pyroxenes. Finally, highly variable Mg# in constituent minerals, typical for ultramafic cumulates from Kharchinsky volcano in northern Kamchatka and considered to be characteristic of a cumulate origin (Bryant et al. 2007), are not found in the Avachinsky veins. Hence, the veins can be interpreted as products of high-pressure crystallization with variable clinopyroxene/orthopyroxene ratios, similar to websterites produced in crystallization experiments of primitive arc magmas (Müntener et al. 2001).

Pyroxene equilibration temperatures indicate that the vein minerals underwent sub-solidus re-equilibration and thus clinopyroxene was not directly in equilibrium with a melt, but with orthopyroxene ± amphibole at sub-solidus temperatures. Since amphibole may contain significant amounts of trace elements, in the following discussion we will only consider the vein AVX-60v, where amphibole is absent and hence sub-solidus re-equilibration of clinopyroxene with amphibole is not relevant. Moreover, clinopyroxene is the major phase in this vein so that incorporation of trace elements in opx is minimal. Although many trace element concentrations in opx are below the detection limit, the measured HREE concentrations (Ho, Er, Lu) agree well with those calculated using cpx-opx partitioning data for 1,300°C (Lee et al. 2007), suggesting that HREE concentrations have not been significantly affected by sub-solidus re-distributions, in agreement with the narrow range of opx–cpx distribution coefficients ($D^{opx/cpx}$) (Eggins et al. 1998). Although LREE have a more pronounced temperature dependence of $D^{opx/cpx}$, orthopyroxene is not a significant repository for highly incompatible trace elements, including the LREE (Eggins et al. 1998). Therefore, melt compositions calculated from clinopyroxene compositions of sample AVX-60v should not be significantly affected by sub-solidus re-equilibration.

The REE and trace element composition of a melt in equilibrium with clinopyroxene from vein AVX-60v was calculated using cpx-hydrous melt partition coefficients from Green et al. (2000) (Fig. 7). The chondrite-normalized REE pattern of this melt has a convex shape and is slightly LREE-enriched $(La/Yb)_N = 2.3$ (Fig. 7a). REE concentrations (1–10× chondrite) are relatively low compared to most primitive arc basalts and andesites (Kelemen et al. 2003). A relative depletion of the MREE is reflected by both high $(La/Sm)_N$ (~ 6.0) and low $(Gd/Yb)_N$ (~ 0.4). Both Kamchatka arc basalts and average continental arc andesites (Kelemen et al. 2003) have higher $(Gd/Yb)_N$ ratios of 1.5 and 2.1, respectively. The REE pattern of the

calculated melt overlaps with those of boninites, and is similar to melts produced by hydrous melting and refertilization of sub-arc mantle peridotite (Bizimis et al. 2000). Further similarities between the calculated melt and boninites are enrichments of Zr–Hf, Sr and Pb compared to elements with similar incompatibility (Fig. 7b). The positive Zr–Hf anomaly is caused by the fact that Zr and Hf are much more incompatible in clinopyroxene than Sm during hydrous melting ($^{Sm}D_{cpx\text{-}melt} = 0.23$ and $^{Zr}D_{cpx\text{-}melt} = 0.043$) (Green et al. 2000).

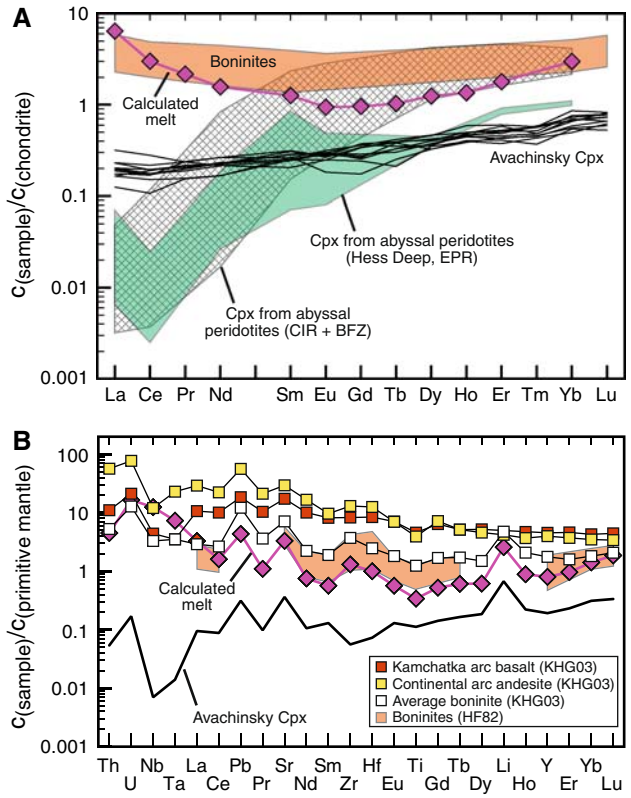

Fig. 7 **a** Chondrite-normalized (Boynton 1984) REE diagrams for clinopyroxenes from metasomatic veins in Avachinsky mantle xenoliths compared to clinopyroxenes from depleted abyssal peridotites from the Central Indian Ridge (CIR) (Hellebrand et al. 2001), the Bouvet Fracture Zone (BFZ) (Johnson et al. 1990) and the East Pacific Rise (EPR) (Dick and Natland 1996). HREE contents of the vein clinopyroxenes are lower than in abyssal peridotites, consistent with depletion due to higher degrees of melting. However, vein clinopyroxenes have less fractionated REE patterns, indicating refertilization as in the hydrous melting and refertilization model from Bizimis et al. (2000). An average melt composition was calculated using clinopyroxene-melt partition coefficients for hydrous melting (experimental run 1787) from Green et al. (2000). The REE pattern of the calculated melt bears similarities to boninites (Hickey and Frey 1982), both in terms of absolute concentrations as well as regarding the convex pattern. **b** Primitive-mantle normalized (McDonough and Sun 1995) trace element diagram of melts calculated from vein clinopyroxene composition. Data sources for partition coefficients: Th, U, Pb, Ti: Ionov et al. (2002); Li: Gaetani et al. (2003); all other elements: Green et al. (2000). Comparative lava compositions: KHG03 = Kelemen et al. (2003); HF82 = Hickey and Frey (1982). Note that the calculated melt compositions has positive Pb, Sr and Li peaks and absolute trace element contents most similar to boninites

A boninitic melt as the source of the pyroxenites is consistent with the sub-arc setting and experimentally determined melting conditions. Boninites, which are relatively primitive arc lavas characterized by high MgO (>8 wt%), high SiO_2 (>53 wt%) and low TiO_2 (<0.5 wt%) contents (Hickey and Frey 1982; Stern et al. 1991), are believed to originate from partial melting of refractory mantle peridotite that has been metasomatically enriched in the presence of at least 1–2 wt% water (Falloon and Danyushevshy 2000). Relatively Si-rich magmas are also required in high-pressure crystallization experiments to produce websterites with variable clinopyroxene/orthopyroxene ratios (Müntener et al. 2001). Naturally occurring orthopyroxene-rich veins and dikes in xenoliths (Bali et al. 2006) and in ophiolites (Tamura and Arai 2006) are interpreted as having formed from boninitic melts traversing and interacting with the mantle. In the case of the Oman ophiolite, the veins are lacking olivine, but contain clinopyroxene with low concentrations of incompatible elements (Tamura and Arai 2006), similar to the veins in the Avachinsky xenoliths.

Boninites occur predominantly in the Izu–Bonin–Mariana arc system (Hickey and Frey 1982; Stern et al. 1991), but recent discoveries include boninitic lavas in ophiolites from northeastern Kamchatka (Osipenko 2003) and boninitic glasses in mantle xenoliths (Koloskov et al. 2001). Hence, it is possible that boninitic magmas are more common in deep regions of the mantle wedge in many convergent margin settings than their abundances in arcs would suggest and boninites could therefore play an important role in the generation of arc magmas. The scarcity of boninites in the Kamchatka arc may reflect continuous reaction of the melts with both the sub-arc mantle and the arc crust during ascent, leading to their chemical modification.

Fluid- versus melt-dominated metasomatic enrichment

The pyroxenite veins in the Avachinsky harzburgite xenoliths formed from a melt, but the spikes of fluid-mobile trace elements suggest the involvement of a metasomatic fluid earlier in their petrogenesis, probably through addition of a metasomatic fluid to the peridotitic source of the parental melt (boninite). In the following discussion, we use the trace element signatures to elucidate the character of the metasomatic agent. Supercritical liquids, which are potentially an important metasomatic agent in subduction zones, are not considered here since they form in mica-rich lithologies of the subducted crust at higher pressures (5–6 GPa) (Kessel et al. 2005), which are not

appropriate for the setting of Avachinsky volcano, where the depth to the slab is approximately 100–120 km, corresponding to ~3–4 GPa.

The trace element concentrations of the veins are determined by the composition of the metasomatic agent, mineral-fluid/melt partition coefficients and sub-solidus re-equilibration. As outlined earlier, sub-solidus re-distribution of trace elements is incapable of producing the high Sr/Nd, Pb/Ce, U/Th and Li/Ho ratios, which also cannot be produced by crystal accumulation. Therefore, comparison with peridotite minerals from other tectonic settings can provide information about which trace element characteristics may be related to the metasomatic agent, and which may be related to the partitioning behavior of a particular element. Moreover, calculated bulk vein compositions provide a better estimate of the metasomatic agent's composition than compositions of individual minerals.

Both clinopyroxene and amphibole from the Avachinsky veins have mantle-normalized trace element patterns that are distinct from those of peridotites from other tectonic settings in terms of both concentrations as well as relative enrichments. Mineral major element compositions, which exert an influence on trace element partitioning behavior (Blundy and Wood 2003), are sufficiently similar between the same minerals from different types of peridotites to suggest that various enrichment spikes (U, Pb, Sr, Li) and troughs (Th, Nb) observed in the trace element patterns reflect the composition of the medium from which the minerals crystallized, and are not a function of the crystal chemistry. For instance, the large positive Pb anomaly is consistent with the preferential extraction of Pb from subducted slabs (Eiler et al. 2007).

In order to compare our data from natural sub-arc mantle to hypothetical slab-derived liquids, we calculated the equilibrium trace element content of slab liquids (fluid and melt) using experimentally determined high-pressure (4 GPa) trace element partitioning data (Kessel et al. 2005) and N-MORB as starting material. Using the batch melting equation

$$c_l = c_o \cdot 1/[D + F(1 - D)],$$

where c_l is the concentration in the liquid, c_o is the original concentration, D is the solid–liquid bulk partition coefficient and F is the weight fraction of liquid produced, we varied the degree of melting (F) between 3 and 30%. Over this range of F, changes in concentrations of the elements Nd to Lu in the liquid are insignificant, and the variability of the elements Rb to Sr remains within one order of magnitude. Since patterns of relative trace element concentrations are insensitive to variations in degree of melting, we focus on the shape rather than the position of model results. Here, a value of $F = 10\%$ was chosen as representative.

Depending on the temperature, either a fluid (700–900°C) or a melt (1,000°C) can be produced at 4 GPa (Fig. 8). In comparison to the bulk veins, all hypothetical liquids are enriched in the majority of trace elements except the HREE (Fig. 8a). The characteristic positive Ba, U, Pb and Sr peaks of the bulk veins are very pronounced in the fluids generated at 700 and 800°C as well, but are relatively small or even negative (Pb) in the liquids produced at higher temperatures. A positive Li peak appears in all hypothetical liquids, similar to the bulk veins. In contrast to the veins, LREE are enriched in the calculated liquids relative to HREE and show a positive correlation between degree of enrichment and temperature. The calculated hydrous melt at 1,000°C has several features that are distinct from the bulk vein chemistry: high LREE concentrations, relative depletion of Pb compared to Ce and enrichment of Nb and Ta compared to Th and U. Trace element contents of the veins and those of the hypothetical melt differ by about two orders of magnitude, which is quite significant. This suggests that the veins cannot be derived solely from slab melting and that metasomatic overprinting of the source region of the veins by slab melts was not significant. Melting of subducted crust would also lead to HREE depletion due to incorporation of HREE in residual garnet, but this is not observed in the bulk vein patterns or in lavas from the southern segment of the Kamchatka arc. Calculated melts from AOC or sediment generally have high concentrations of Nb, REE and Zr (Eiler et al. 1998). Hence, the observed low concentrations of these elements point to a depleted, peridotitic source, as suggested for phonolitic glass inclusions in mantle olivine (Eiler et al. 1998).

In contrast, calculated fluid compositions, in particular those at 700 and 800°C, show many similarities in their patterns to the bulk veins (Fig. 8). Since Ba, Pb, Sr, U and K are fluid-mobile relative to HFSE (Brenan et al. 1995; Keppler 1996), mantle rocks metasomatized by aqueous fluids are expected to be characterized by high Ba/Th, U/Th, U/Nb and Pb/Ce ratios (Eiler et al. 2007; Keppler 1996; Kessel et al. 2005; Stalder et al. 1998). Characteristics of slab-derived fluids also include relatively high concentrations of LREE, MREE and Sr, but low concentrations of HREE and Ti (Bizimis et al. 2000, Savov et al. 2007). The major enrichments (U, Pb, Sr, Li) of the bulk vein compositions as well as the relative depletion in Nb and Ta are consistent with a fluid origin, based on the fluid–rock partitioning behavior.

Ratios of relatively fluid-mobile (Pb, Sr) trace elements versus REE of similar incompatibility provide a means to compare fluid- versus melt-induced trace element signatures in more detail. Bulk veins as well as various arc lavas, including those from Avachinsky (Ishimaru et al. 2007; Kelemen et al. 2003), lie on a trend between N-MORB and

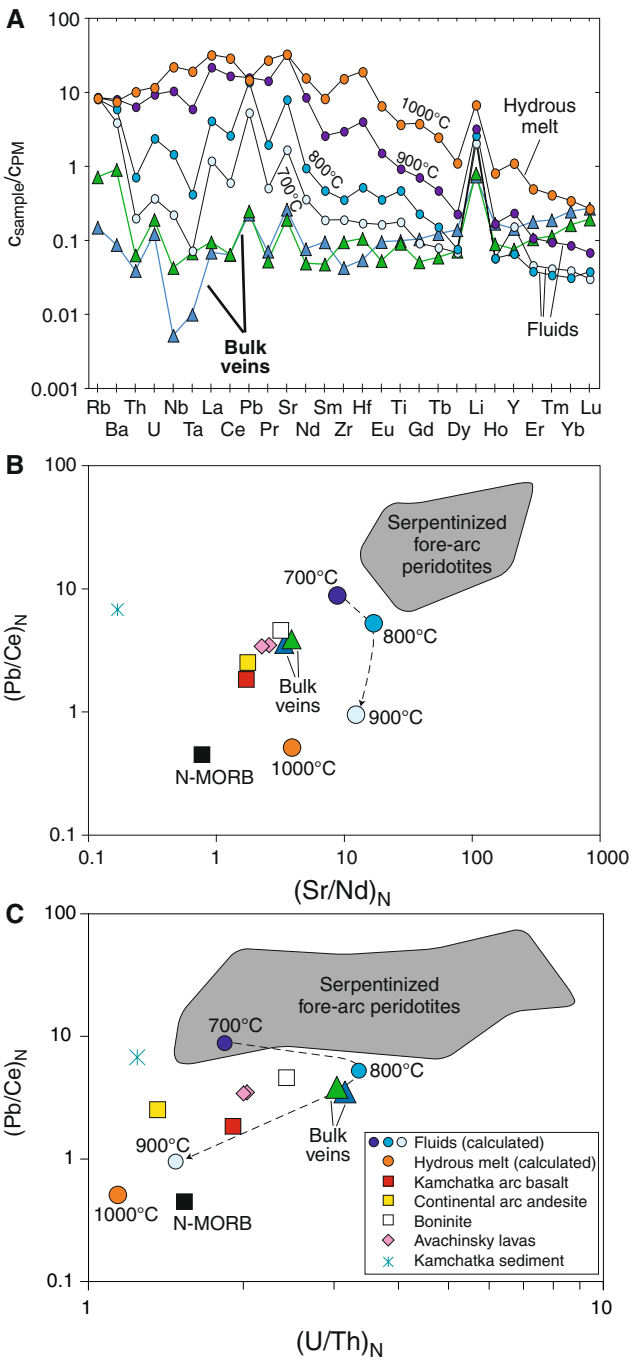

Fig. 8 Primitive mantle-normalized (McDonough and Sun 1995) trace element diagrams for metasomatic veins from Avachinsky mantle xenoliths showing fluid-inherited signatures. **a** Calculated bulk vein compositions (*blue triangles* AVX-60v, *green triangles* AVX-61v) compared to calculated fluid and melt compositions. Fluid and melt compositions were calculated based on liquid-bulk rock partition coefficients (Kessel et al. 2005) using N-MORB (Sun and McDonough 1989) as starting material and assuming 10% batch melting. **b** $(Pb/Ce)_N$ versus $(Sr/Nd)_N$ and **c** $(Pb/Ce)_N$ versus $(U/Th)_N$ trace element ratio diagrams for calculated bulk vein, slab fluid and melt compositions, various arc lavas (Kelemen et al. 2003), serpentinized fore-arc peridotites (Savov et al. 2005), Kamchatka sediment (Plank and Langmuir 1998) and N-MORB (Sun and McDonough 1989). Note that bulk veins and most arc lavas plot on trends between N-MORB and slab fluid compositions calculated using partition coefficient data for 700–800°C (Kessel et al. 2005). Bulk veins do not show similarities with the calculated hydrous melt and the Kamchatka sediment

fluid compositions calculated for 700–800°C on plots of $(Sr/Nd)_N$ versus $(Pb/Ce)_N$ (Fig. 8b) and $(U/Th)_N$ versus $(Pb/Ce)_N$ (Fig. 8c). The data trend toward the composition of serpentinized fore-arc peridotites that have been infiltrated by subduction zone fluids (Savov et al. 2005). This suggests that the relative enrichments in Pb, Sr and U observed in the veins are inherited from a slab-derived fluid. In combination with the otherwise mostly low trace element contents of the bulk veins, a scenario whereby an initially depleted mantle source is modified by small additions of slab-derived components transported by the metasomatic fluid (Eiler et al. 2007) appears appropriate. This fluid has a negative Nb–Ta trough, positive Sr and Pb peaks, and $U_N > Th_N$. Taking the trends at face value, the temperature of the slab-derived fluid was likely to be in the 700–800°C range.

To obtain a more complete picture of the slab to arc transfer processes, it is important to tie in the constraints from the metasomatic veins with what has been learned from xenoliths and arc lavas in the southern segment of the Kamchatka arc and Avachinsky, in particular. The bulk-rock geochemistry of Avachinsky mantle xenoliths is characterized by negative Ta anomalies, enrichments in LILE (Ba and U) relative to HFSE and REE, and elevated LREE/HREE ratios (Ishimaru et al. 2007; Kepezhinskas and Defant 1996). These geochemical features are characteristic for almost all island arc volcanic rocks (Gill 1981; Hawkesworth et al. 1993), including samples from Avachinsky volcano (Kepezhinskas et al. 1997; Turner et al. 1998). Hence, this suggests that the sub-arc mantle has been affected by metasomatic processes that changed the geochemistry in a direction toward what is observed in Avachinsky host lavas.

The harzburgite xenoliths are more depleted than the presumed MORB mantle composition, both in terms of bulk chemical and mineralogical compositions (Kepezhinskas et al. 2002), suggesting a hydrous melting scenario, where a constant fluid flux in the mantle wedge causes large depletions in the more fusible major elements (Al, Ca) and incompatible trace elements (Bizimis et al. 2000). The low Ti and HREE contents in the Avachinsky vein clinopyroxenes, with HREE concentrations lower than those seen in cpx from abyssal peridotites (Fig. 7), also indicates large degrees of melting in the melt source rocks. However, LREE/HREE ratios of the harzburgites are higher than in abyssal peridotites, suggesting re-enrichment of the LREE caused by the flux of a slab-derived fluid, in

which Ti and HREE are not soluble. HREE contents of the melts that produced that pyroxenite veins are controlled by the degree of melt depletion of the source, whereas LREE contents are controlled by the fluid (Bizimis et al. 2000).

Trace element and Sr–Nd–Pb–Os isotope data for lavas and mantle xenoliths were used to argue that modification of the mantle wedge in the southern Kamchatka arc segment, where Avachinsky is located, is caused by fluids (Kepezhinskas et al. 2002; Kepezhinskas et al. 1997; Saha et al. 2005; Widom et al. 2003). Moreover, hydration of the mantle wedge by fluids is suggested by thermal models of the Kamchatka arc (Manea and Manea 2007). There is also a pronounced similarity between the composition of the metasomatic fluid, as inferred from the Avachinsky veins, and the slab component determined from volcanic front lavas at the Mutnovsky volcano, which show peaks for Sr, Pb and Li, troughs for Nb and Ta, and enrichment of U and Ba over Th on N-MORB normalized trace element diagrams (Duggen et al. 2007). In summary, the pyroxenite veins in the Avachinsky xenoliths crystallized from a melt, similar in composition to boninite, that was generated by slab fluid-fluxed melting of the sub-arc mantle.

Li geochemistry of metasomatic agents in the sub-arc mantle

Lithium is a fast diffusing element (Coogan et al. 2005; Giletti and Shanahan 1997; Richter et al. 2003) and inter-mineral Li isotopic disequilibria in mantle xenoliths can be caused by Li ingress during interaction of the xenoliths with host magmas (Aulbach and Rudnick 2009; Aulbach et al. 2008; Jeffcoate et al. 2007; Rudnick and Ionov 2007) or during slow cooling (Ionov and Seitz 2008; Gao et al. 2008). The Avachinsky xenoliths lack evidence for infiltration of host magma into the xenolith, and, most importantly, their minerals are in isotopic equilibrium (see also Ionov and Seitz 2008). In addition, since the Avachinsky host lavas have significantly higher Li concentrations than the xenoliths, their Li concentrations are not related to their entrainment in the host rock. Thus, these xenoliths likely reflect the Li elemental and isotopic signatures of the sub-arc mantle.

Li elemental and isotopic equilibrium between olivine and orthopyroxene in the harzburgites, as well as between olivine and vein pyroxenes, indicate that either the metasomatic agent was not isotopically different from the surrounding mantle or that the distinctive Li isotope composition of the slab-derived fluid was obliterated by diffusion. In the following section, we first evaluate the Li signatures of potential slab fluids, and then calculate whether diffusive equilibration is a viable mechanism to explain the observed mantle-like Li isotopic composition and equilibration seen in the xenoliths.

Most arc lavas have Li isotopic compositions similar to MORB (and OIB) and do not show systematic cross-arc variations. Therefore, it has been proposed that the sub-arc mantle may act as a chromatographic column, where Li released from the slab is retained in mantle minerals (Tomascak et al. 2000). During subduction, fluids released from the slab are enriched in Li due to its partitioning into fluids at metamorphic conditions (Benton et al. 2004; Brenan et al. 1998b; Wunder et al. 2006). Major Li-bearing minerals in high-pressure, subduction-related metamorphic rocks are chlorite, glaucophane, clinopyroxene, phengite, paragonite and staurolite (Marschall et al. 2006; Wunder et al. 2007). These phases contain more than 95% of the Li budget (Marschall et al. 2006) and their breakdown gives rise to elevated Li concentrations in the released fluids. Moreover, Li abundances in the subducted slab inventory [$\sim$10–36 ppm for Pacific AOC (Kelley et al. 2003) and 12–80 ppm for Pacific sediments (Chan et al. 2006a)] are large compared to the amount of Li in typical peridotite ($\sim$1.6–1.8 ppm) (Ottolini et al. 2004).

Slab-derived fluids are expected to be enriched in ^{7}Li due to the preference of the heavier isotope for the fluid phase during serpentinization and slab dehydration (Wunder et al. 2006). Evidence for this comes from fore-arc pore waters from serpentinite seamounts (Benton et al. 2004; Chan et al. 2006b; Savov et al. 2002). At greater depths, however, fluids may become isotopically light because the slab becomes depleted in ^{7}Li (Zack et al. 2003; Marschall et al. 2007) and Li stable isotope fractionation decreases due to higher temperatures (Wunder et al. 2006). Thus, interaction with isotopically variable, Li-rich fluids should be reflected in distinctive Li isotopic compositions and elevated Li concentrations.

During partial melting, Li is moderately incompatible ($D^{Li}_{mineral\text{-}melt} = 0.13$–$0.35$) (Brenan et al. 1998a) and Li isotopic fractionation is inferred to be negligible (Halama et al. 2007; Tomascak et al. 1999). Thus, melts should reflect the isotopic composition of their source. Sediment melts may be isotopically variable, reflecting the variability of δ^{7}Li in deep-sea sediments ($\delta^{7}Li = -4$ to $+15$) (Bouman et al. 2004; Chan et al. 2006a). The AOC also exhibits a considerable range in δ^{7}Li from -2 to $+21$ (Bouman et al. 2004; Chan et al. 1992, 2002), but is commonly heavier (weighted average of 11.3; Elliott et al. 2006) than fresh MORB ($\delta^{7}Li = 3.4 \pm 1.4$) (Tomascak et al. 2008) due to the preferential incorporation of ^{7}Li from seawater. Melts derived from metabasalts are likely to be isotopically light due to an, on average, negative δ^{7}Li value of eclogites (-1.6 ± 2.0) (Marschall et al. 2007).

Our Li isotope data show that there is no significant difference between the MORB mantle and the metasomatized sub-arc mantle as sampled by the investigated xenoliths from the Kamchatka arc. In combination with the

lack of significant inter-mineral elemental and isotopic disequilibria and with MORB-like δ^7Li values (0 to +5) found in vein-free Avachinsky mantle xenoliths (Ionov and Seitz 2008), we conclude that the shallow sub-arc mantle above the zone of arc magma generation is similar to the MORB mantle in terms of Li isotopic composition, despite evidence for modal metasomatism, including Li addition, and the Li isotopic variability potentially induced by slab-derived agents.

A relative enrichment of Li compared to the HREE occurs in metasomatic clinopyroxene (Li/Yb ~8), orthopyroxene (Li/Yb ~41), and calculated bulk vein compositions. However, the absolute Li concentrations in the vein minerals are similar to typical mineral concentrations in fertile and depleted mantle (Seitz and Woodland 2000) (Fig. 5). Amphibole does not show a Li versus HREE enrichment, but clinopyroxene and amphibole appear to be in Li elemental equilibrium since the apparent Li distribution coefficient between clinopyroxene and amphibole is ~0.9, which is within the range of distribution coefficients that have been determined for other rocks [$^{Li}D_{cpx\text{-}amph}$ = 0.06–1.66 in alkaline igneous rocks (Marks et al. 2004) and 0.04–1.2 in high-pressure metamorphic rocks (Marschall et al. 2006)].

The hydrous flux melting and refertilization model of Bizimis et al. (2000) can explain enrichment of fluid-mobile elements (like Li) in the mantle wedge compared to immobile elements of similar incompatibility. Flux melting leads to the removal of incompatible elements in the mantle, but fluid-mobile elements are replenished due to the constant fluid flux (Bizimis et al. 2000). In the case of the Avachinsky veins, this geochemical signature could have been inherited from previous flux melting and refertilization events in the deeper parts of the mantle wedge where initial melting took place. Hence, elevated Li/Ho ratio is predominantly due to the removal of HREE during multiple hydrous melting events in the mantle wedge and replenishment of Li via fluid fluxing post-dating the melting, before the vein-forming melt was generated. The lack of a Li peak in amphibole is probably related to its preference for HREE compared to clinopyroxene (Adam and Green 2006).

Diffusive Li equilibration in the sub-arc mantle

The sub-arc mantle may have incorporated large heterogeneities in Li concentrations and δ^7Li values from slab-derived metasomatizing agents (Benton et al. 2004). The trace element patterns of the metasomatic veins in the Avachinsky xenoliths provide evidence for fluid-dominated metasomatism. Whether a subduction zone signature in δ^7Li can be carried across the mantle wedge depends on the speed and mechanisms of melt transport and Li diffusive equilibration.

Li diffusion is an important process controlling mantle Li budgets (Beck et al. 2006; Parkinson et al. 2007; Richter et al. 2003; Rudnick and Ionov 2007). If we assume that the metasomatic veins had initially higher Li concentrations than the harzburgites, then the similar δ^7Li values and Li abundances in harzburgites and metasomatic veins can be used to calculate a minimum time for which the xenoliths must have resided in the upper mantle, experiencing Li diffusion, prior to their entrainment in the host lava. To model diffusive equilibration, we use an equation describing diffusion out of a cylinder (Crank 1975), where the diffusing substance is initially distributed uniformly through the cylinder:

$$C = C_o \cdot \left[1 - e^{\left(-\frac{a^2}{4Dt}\right)}\right],$$

where C_o is the initial Li concentration of the cylinder, reflecting [Li] in the vein, C is the concentration at the center of the cylinder, a (m) is the radius of the cylinder, D (m^2 s^{-1}) is the diffusion coefficient and t (s) is time. The diffusion coefficients are taken from the experimentally determined best-fit expression for Li diffusion in clinopyroxene (Coogan et al. 2005). Since Li diffusion in orthopyroxene and amphibole has not been determined experimentally, we use Li diffusivity in clinopyroxene as representative of the metasomatic veins.

At temperatures of 1,000°C, the minimum time that small pyroxenite veins (width ~1–2 cm) would need to fully equilibrate is only on the order of a few 100 years (Fig. 9). Even at a relatively low temperature of 800°C the veins would equilibrate with the mantle peridotite in less than 10^5 years. However, in this dynamic environment, it is unlikely to maintain such a constant and low temperature condition for long time periods. Thus, on a geological time scale, Li diffusive equilibration in the sub-arc mantle is a rapid process, and it is clear from the modeling that metasomatic veins like those in the Avachinsky xenoliths can easily equilibrate with the mantle peridotite. Moreover, it is likely that some Li equilibration already occurred during melt ascent in the wedge prior to vein crystallization. We concur with Rudnick and Ionov (2007), who concluded that if Li zoning occurs in mantle xenoliths, it must be a recent event. The absence of Li zoning in the veined xenoliths suggests that they resided in the mantle for 10–10^5 years before they were carried to the surface.

Diffusive equilibration can also explain why there is a relative enrichment of Li compared to the HREE in the veins, but no absolute enrichment in Li compared to typical mantle minerals or the surrounding harzburgite. HREE depletion in the veins reflects the low HREE concentration in the parental (boninitic) melt, which was generated by intense flux melting in deeper mantle regions. This melt was enriched in Li, but depleted in HREE. Whereas

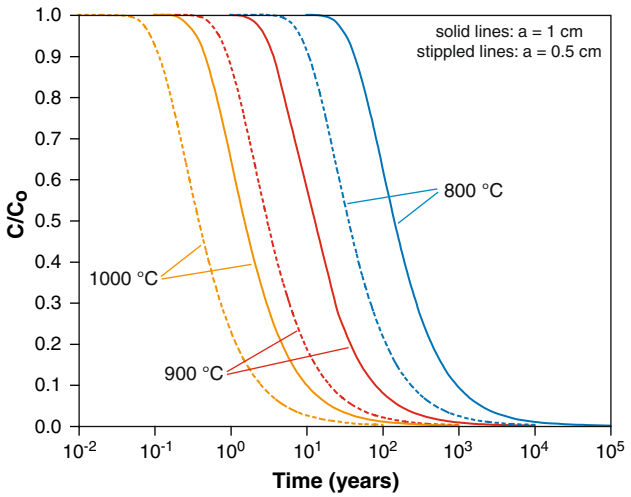

Fig. 9 Li diffusion modeling for a cylindrical vein with an elevated Li concentration (20 ppm) within the mantle. For simplicity, the Li concentration in the surrounding mantle is assumed to be zero. C_o is the uniform concentration in the cylinder initially, and C is the concentration at the center of the cylinder. Hence, the axis $r = 0$ is considered, so that equation 3.11 from Crank (1975) for the diffusion of a cylinder of solute into a large volume of solvent can be applied. Diffusion coefficients used in the calculation are those calculated using the best fit Arrhenius expression given in Coogan et al. (2005): $D = 8.0 \times 10^{-15}$ at 800°C, 9.4×10^{-14} at 900°C, 7.5×10^{-13} at 1,000°C (values in m^2/s). *Curves* are shown for radii of the cylindrical model veins of 0.5 and 1 cm. With increasing equilibration, C/C_o is approaching zero

concentrations of HREE, which have low diffusivities (van Orman et al. 2001), remained low in the vein minerals, fast diffusing Li equilibrated with the surrounding mantle. Therefore, Li concentrations likely decreased in the vein minerals, which now exhibit Li concentrations typical for mantle minerals, but they are still higher than those of the depleted HREE.

Implications for Li cycling in subduction zones

Our results and the data from Ionov and Seitz (2008) suggest that it is unlikely that a strongly fractionated Li isotope signature in slab fluids can survive dilution through interaction with the mantle wedge, since rapid Li diffusion causes Li buffering of ascending fluids and melts with the peridotitic wall rock. Further evidence for the buffering capacity of the sub-arc mantle for slab-derived Li is indicated by the general overlap in δ^7Li between MORB and arc lavas (Tomascak et al. 2002). To determine the degree to which the Kamchatka sub-arc mantle is capable of buffering the Li flux from the slab, we calculated the amount of Li that is potentially released from the slab (Table 4). We assume that a section of 0.35 km sediment (Plank and Langmuir 1998), 7 km oceanic crust and 5 km serpentinized mantle is completely subducted at a subduction angle of 55° (Gorbatov et al. 1997) and a subduction rate of 90 mm/year (Plank and Langmuir 1998). This section constitutes the source for all subducted Li (Fig. 10a). In our model, the serpentinized mantle is meant to include mantle wedge serpentinite and hydrated slab mantle (Straub and Layne 2003). Although Ranero et al. (2003) proposed that the latter may reach considerable thickness (up to 30 km), the variable degree of serpentinization is decreasing with depth and unlikely to be > 20% because fully serpentinized peridotite with a density of ~2.5 g/cm^3 would be almost unsubductable (Ernst 1999). Moreover, geochemical data from the Izu arc suggest that the lithospheric serpentinite does not contribute significant amounts of fluid to the arc (Straub and Layne 2003). Thus, the 5 km of serpentinized mantle assumed here are likely to be in the upper range of both mantle wedge and lithospheric serpentinite sources of Li.

Assuming that ~30% of the total amount of subducted water is released in the 80–150 km depth-to-the-slab interval (Schmidt and Poli 2003), accounting for 24% of the subducted Li, as ~1/5 of Li remains in minerals (Brenan et al. 1998b), about 5×10^{11} kg Li will be released in a 100 km wide segment of the volcanic arc. The slab length in the chosen depth interval (~85 km) is very similar to the slab subducted in 1 Ma (90 km), so that the Li flux off the slab can be approximated as 5×10^{11} kg/Ma, corresponding to 2.3 mol/s. Assuming a mantle convection speed similar to the subduction rate, we calculated that 1.2×10^{12} kg/Ma (5.5 mol/s) of Li stored in peridotite minerals passes through the convecting part of the mantle beneath the arc. Hence, the convecting mantle wedge alone appears to be capable of buffering significant amounts of Li released from the slab. On the other hand, if 10% of the slab-derived Li passes unaffected through the wedge and reaches the lithospheric part of the sub-arc mantle, it will take only ~17 million years until the slab-derived Li dominates the budget in the lithospheric mantle. The fact that there is no significant difference in δ^7Li between the lithospheric sub-arc mantle in a mature subduction zone like Kamchatka and global estimates of the mantle Li isotopic composition suggests that most of the Li flux from the slab equilibrates with the convecting mantle wedge. Hence, the overall Li flux into the lithospheric mantle will not impart a highly fractionated Li isotopic signature, possibly aided by the balancing of isotopically heavy reservoirs (AOC and aqueous fluids) with isotopically light Li reservoirs (sediments and eclogites).

The evidence for complete Li isotope equilibration between the veins and the surrounding harzburgite from the Kamchatka xenoliths is important for understanding Li cycling in subduction zones and the thermal state of the sub-arc mantle (Fig. 10b). In the fore-arc part of the mantle wedge, Li isotope studies of serpentinite mud volcanoes

Table 4 Parameters used and results calculated for the Li subduction flux

Parameter	Value	Data source
Subduction angle	55°	Gorbatov et al. (1997)
Subduction rate	90 mm/year	Plank and Langmuir (1998)
Thickness continental crust	37 km	Levin et al. (2002)
Length of arc segment	100 km	
Oceanic sediments		
Thickness	0.35 km	Plank and Langmuir (1998)
Density	1.64 g/cm^3	Plank and Langmuir (1998)
Li concentration	25 ppm	Bouman et al. (2004)
Volume	3.0×10^{15} km^3	
Calculated Li mass	1.2×10^{11} kg	
Oceanic crust		
Thickness	7 km	Kelemen et al. (2003)
Density	3.0 g/cm^3	Kelemen et al. (2003)
Li concentration	10 ppm	Chan et al. (1992), Bouman et al. (2004)
Volume	6.0×10^{16} km^3	
Calculated Li mass	1.8×10^{12} kg	
Serpentinized slab mantle		
Thickness	5 km	Schmidt and Poli (2003)
Density	2.975 g/cm^3	Schwartz et al. (2001)
Li concentration	2.45 ppm	Savov et al. (2007)
Volume	3.1×10^{16} km^3	
Calculated Li mass	2.2×10^{11} kg	
Sub-arc mantle		
Density	3.4 g/cm^3	Savov et al. (2007)
Li concentration	1.6 ppm	McDonough and Sun (1995)
Thickness lithospheric mantle	33 km	Nizkous et al. (2006)
Volume lithospheric mantle	1.6×10^{17} km^3	
Li mass lithospheric mantle	8.8×10^{11} kg	
Volume convecting mantle	2.2×10^{17} km^3	
Li mass convecting mantle	1.2×10^{12} kg	
Depth-to-slab segment	80–150 km	
Water released from slab	30%	Schmidt and Poli (2003)
D_{Li} mineral-fluid	0.2	Brenan et al. (1998a)
Li released from slab	24%	
Mass of Li released	5.1×10^{11} kg	

reveal that the Li budget is controlled by fluid interaction at relatively low temperatures (<300°C) (Benton et al. 2004; Savov et al. 2007), i.e., Li diffusion has little influence. Slab rocks from depths of approximately 60 km, where eclogitization takes place, record complex Li elemental and isotopic variations. These are caused by dehydration, diffusion and further modifications during uplift (Marschall et al. 2007; Zack et al. 2003), thus masking the Li geochemical signatures of the original slab fluids. At depths of 100–120 km, our data and the study by Ionov and Seitz (2008) show that Li elemental and isotopic variability from slab-derived agents is not preserved in the sub-arc mantle because of rapid Li diffusion. Hence, there appears to be a vertical transition in the wedge from the fore-arc region, where high fluid–rock ratios and low temperatures allow preservation of the slab flux signature, to the sub-arc region, where Li diffusion is the dominant process, obliterating any variability derived from the slab. Such a vertical boundary between cold and relatively hot regions in the wedge and the existence of a "cold nose" have also been proposed based on attenuation tomography at a slab depth of 80 km (Abers et al. 2006). Thermal modeling (Abers et al. 2006; Manea and Manea 2007) and the geothermometry of the sub-arc xenoliths indicate that temperatures at depths of ~50 km are on the order of 900–1,100°C, i.e., high enough to enable effective Li diffusion. Hence, mature arc settings are unlikely to record Li isotopic variability in either lavas or mantle xenoliths. Only in

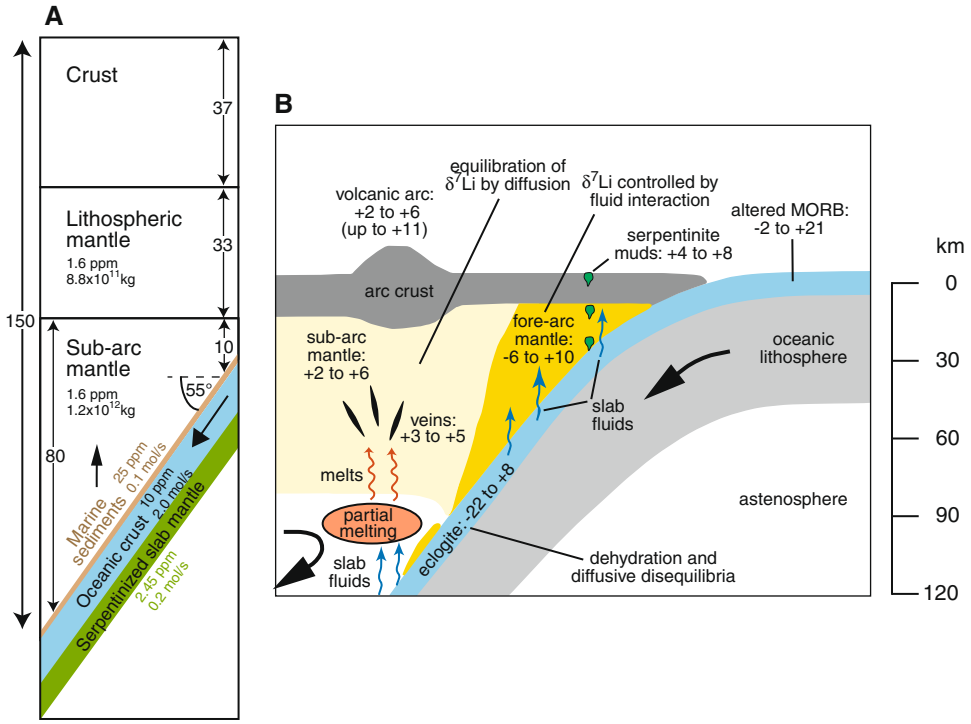

Fig. 10 **a** Schematic sketch showing the geometry used for the Li flux calculation in the Kamchatka arc with Li concentrations (in ppm), Li flux off the slab units (in mol/s) and total mass of Li present in the mantle (in kg) given. *Numbers at arrows* denote the distance (in km). **b** Schematic illustration of Li isotope systematics in a subduction zone (modified after Zack et al. 2003). In altered MORB and in the fore-arc mantle, δ^7Li values are controlled by fluid interaction and hence highly variable with a tendency to high values. In contrast, at higher temperatures in the sub-arc mantle, Li isotopic equilibration occurs via diffusion. δ^7Li in eclogites is influenced by both diffusion and dehydration processes, but temperature and time are not sufficient to allow the rocks to re-equilibrate. δ^7Li values for serpentinite muds and peridotite clasts from the fore-arc are from Benton et al. (2004) and values for eclogites are from Marschall et al. (2007)

unusual geotectonic circumstances might a significant variability in δ^7Li in arc lavas be observed. For instance, calc-alkaline and ultrapotassic lavas from Anatolia erupted during the transition from orogenic to intraplate magmatism show highly variable δ^7Li values related to the effects of a dying slab (Agostini et al. 2008). In contrast, fluid-fluxed melting of the mantle was invoked to explain elevated δ^7Li values in arc lavas from Panama (Tomascak et al. 2000). These results can be reconciled with the Avachinsky data if we allow material from the "cold nose", which records high fluid–rock ratios, to be transported into deeper mantle regions without fully equilibrating in terms of Li and thus preserving Li heterogeneities when this material melts. The vast majority of arc lavas, however, record MORB-like Li isotopic signatures, consistent with the implication of the Avachinsky data (Ionov and Seitz 2008; this study) that slab Li is buffered by diffusive equilibrium in the middle and upper parts of the sub-arc mantle, thus obliterating any slab isotopic signature.

A simplified scenario for Li transfer beneath arcs can be outlined as follows: fluids with variable δ^7Li and high Li contents are continuously released from the subducted slab at depths of about 100–120 km. As these fluids infiltrate the mantle wedge, they trigger melting. A constant fluid flux leads to sustained melting episodes, thereby depleting the mantle wedge. However, the fluid flux also leads to a re-enrichment in fluid-mobile trace elements, similar to the hydrous melting and refertilization model of Bizimis et al. (2000). The initial melts resemble boninites (i.e., are derived from refertilized refractory mantle sources), but also carry diagnostic trace element features of slab fluids. During ascent, these boninite-like melts are modified by assimilation and crystal fractionation. Remnants of these melts form pyroxenitic veins, as observed in the Avachinsky mantle xenoliths. The high diffusivity of Li causes δ^7Li and Li contents of the melts and veins, respectively, to equilibrate with the surrounding mantle peridotite over relatively rapid timescales ($<10^3$ to 10^4 years), so that both δ^7Li and Li concentrations of the veins resemble those of the surrounding mantle ($\delta^7\text{Li} = +3$ to $+5$, [Li] = 1–2 ppm).

Conclusions

Pyroxenite veins in harzburgite xenoliths from Avachinsky volcano, Kamchatka, crystallized from a melt with

compositional similarities to boninites that bore the trace element signature (high Ba/Th, U/Th, Pb/Ce, Sr/Nd and Li/Ho) of a slab fluid. Although the veins have high Li/HREE (Li/Ho), the absolute concentration of Li in the metasomatic veins is not higher than in the surrounding mantle. Li enrichment relative to HREE in the parental melt to the veins was probably produced by fluid-fluxed melting in the mantle wedge, where extreme depletion in HREE was caused by continuous fluid-induced melting and fluid-mobile elements were constantly replenished by the fluid flux. The veins and harzburgites are in Li isotopic and elemental equilibrium, and have δ^7Li values similar to MORB and the convecting upper mantle, overlapping the δ^7Li of Avachinsky basaltic andesites. These observations suggest that entrainment of the xenoliths and subsequent cooling had little effect on the δ^7Li of the minerals in the xenoliths, consistent with previous studies of xenoliths from this locality (Ionov and Seitz 2008).

Interestingly, neither the metasomatic veins nor the arc lavas record the fractionated Li isotopic signatures that might be expected of a slab fluid, yet a slab fluid imprint is clearly visible in the trace element signatures of the veins. We suggest that diffusive equilibration of Li with the surrounding mantle occurs in the ascending melts as well as after vein crystallization. Modeling of diffusive Li equilibration at mantle temperatures shows that Li elemental and isotopic equilibrium is achieved within 10–10^5 years. Hence, even if fluids with strongly fractionated Li isotopic signatures were added to the sub-arc mantle, their distinctive signatures are erased as Li equilibrates diffusively over relatively short time scales. Calculations of the flux of Li from the slab and Li equilibration in the Kamchatka sub-arc mantle suggest that the convecting mantle wedge can buffer significant amounts of slab-derived Li, thus limiting the flux of fractionated Li to lithospheric mantle and overlying crust.

In agreement with geophysical observations, the Li data suggest that there is a vertical boundary in the mantle wedge, separating a slab-fluid controlled and relatively cold fore-arc region from a diffusion-controlled, hotter area beneath the arcs. Only the physical transport of cold segments of mantle wedge from the "cold nose" to beneath the arc may enable the incorporation of unusually heavy Li isotopic signatures into volcanic arc rocks.

Acknowledgments The help of Richard Ash with laser ICP-MS analyses is greatly appreciated. We also thank Mary Horan and Timothy Mock for guidance during preparation and acquisition of the Sr isotope data and Heiner Taubald for help with the whole-rock major element analyses. Phil Piccoli, Christos Hadidiacos and Barbara Mader assisted with microprobe measurements. Jeffrey G. Ryan and Steve Shirey contributed to the development of some of the ideas expressed in this contribution, and Jessica Warren expertly assisted in assessing comparative data from abyssal peridotites. We are grateful to Paul Tomascak and Shoji Arai for constructive reviews and to Jochen Hoefs for editorial handling. R. H. acknowledges a Feodor-Lynen fellowship from the Alexander-von-Humboldt Foundation during his time at the University of Maryland and I. P. S. acknowledges fellowship support from the Department of Terrestrial Magnetism of the Carnegie Institution of Washington. This work was supported by NSF grant EAR 0609689 to RLR and WFM. This publication is contribution no. 159 of the Sonderforschungsbereich 574 at Kiel University.

References

Abers G, van Keken PE, Kneller EA, Ferris A, Stachnik JC (2006) The thermal structure of subduction zones constrained by seismic imaging: implications for slab dehydration and wedge flow. Earth Planet Sci Lett 241:387–397. doi:10.1016/j.epsl.2005.11.055

Adam J, Green DH (2006) Trace element partitioning between mica- and amphibole-bearing garnet lherzolite and hydrous basanitic melt: 1. Experimental results and the investigation of controls on partitioning behaviour. Contrib Mineral Petrol 152:1–17. doi:10.1007/s00410-006-0085-4

Agostini S, Ryan JG, Tonarini S, Innocenti F (2008) Drying and dying of a subducted slab: coupled Li and B isotope variations in Western Anatolia Cenozoic Volcanism. Earth Planet Sci Lett 272:139–147. doi:10.1016/j.epsl.2008.04.032

Arai S, Ishimaru S (2008) Insights into petrological characteristics of the lithosphere of mantle wedge beneath arcs through peridotite xenoliths: a review. J Petrol 49:665–695. doi:10.1093/petrology/egm069

Arai S, Ishimaru S, Okrugin VM (2003) Metasomatized harzburgite xenoliths from Avacha volcano as fragments of mantle wedge of the Kamchatka arc: implication for metasomatic agent. Isl Arc 12:233–246. doi:10.1046/j.1440-1738.2003.00392.x

Aulbach S, Rudnick RL (2009) Origins of non-equilibrium lithium isotopic fractionation in xenolithic peridotite minerals: examples from Tanzania. Chem Geol 258:17–27. doi:10.1016/j.chemgeo.2008.07.015

Aulbach S, Rudnick RL, McDonough WF (2008) Li-Sr-Nd isotope signatures of the plume and cratonic lithospheric mantle beneath the margin of the rifted Tanzanian Craton (Labait). Contrib Mineral Petrol 155:79–92. doi:10.1007/s00410-007-0226-4

Bali E, Falus G, Szabó C, Peate DW, Hidas K, Török K, Ntaflos T (2006) Remnants of boninitic melts in the upper mantle beneath the central Pannonian Basin? Mineral Petrol 90:51–72. doi:10.1007/s00710-006-0167-z

Ballhaus C, Berry RF, Green DH (1991) High pressure experimental calibration of the olivine-orthopyroxene-spinel oxygen geobarometer: implications for the oxidation state of the upper mantle. Contrib Mineral Petrol 107:27–40. doi:10.1007/BF00311183

Beck P, Chaussidon M, Barrat JA, Gillet P, Bohn M (2006) Diffusion induced Li isotopic fractionation during the cooling of magmatic rocks: the case of pyroxene phenocrysts from nakhlite meteorites. Geochim Cosmochim Acta 70:4813–4825. doi:10.1016/j.gca.2006.07.025

Benton LD, Ryan JG, Savov IP (2004) Lithium abundance and isotope systematics of forearc serpentinites, Conical Seamount, Mariana forearc: insights into the mechanics of slab-mantle exchange during subduction. Geochem Geophys Geosyst 5(8):Q08J12. doi:10.1029/2004GC000708

Bizimis M, Salters VJM, Bonatti E (2000) Trace and REE content of clinopyroxenes from supra-subduction zone peridotites. Implications for melting and enrichment processes in island arcs. Chem Geol 165:67–85. doi:10.1016/S0009-2541(99)00164-3

Blundy J, Wood B (2003) Partitioning of trace elements between crystals and melts. Earth Planet Sci Lett 210:383–397. doi:10.1016/S0012-821X(03)00129-8

Bouman C, Elliott T, Vroon PZ (2004) Lithium inputs to subduction zones. Chem Geol 212:59–79. doi:10.1016/j.chemgeo.2004.08.004

Boynton WV (1984) Geochemistry of the rare earth elements: meteorite studies. In: Henderson P (ed) Rare earth element geochemistry. Elsevier, Amsterdam, pp 63–114

Braitseva OA, Bazanova LI, Melekestsev IV, Sulerzhitskiy LD (1998) Large Holocene eruptions of Avacha volcano, Kamchatka (7200–3500 14C years B.P.). Volcanol Seismol 20:1–27

Brenan JM, Shaw HF, Phinney DL, Ryerson FJ (1995) Experimental evidence for the origin of lead enrichment in convergent-margin magmas. Nature 378:54–56. doi:10.1038/378054a0

Brenan JM, Neroda E, Lundstrom CC, Shaw HF, Ryerson FJ, Phinney DL (1998a) Behaviour of boron, beryllium, and lithium during melting and crystallization: constraints from mineral-melt partitioning experiments. Geochim Cosmochim Acta 62:2129–2141. doi:10.1016/S0016-7037(98)00131-8

Brenan JM, Ryerson FJ, Shaw HF (1998b) The role of aqueous fluids in the slab-to-mantle transfer of boron, beryllium, and lithium during subduction: experiments and models. Geochim Cosmochim Acta 62:3337–3347. doi:10.1016/S0016-7037(98)00224-5

Brey GP, Köhler T (1990) Geothermometry in four-phase lherzolites II. New thermobarometers, and practical assessment of existing thermobarometers. J Petrol 31:1353–1378

Bryant JA, Yogodzinski GM, Churikova TG (2007) Melt-mantle interaction beneath the Kamchatka arc: evidence from ultramafic xenoliths from Shiveluch volcano. Geochem Geophys Geosyst 8(4):Q04007. doi:10.1029/2006GC001443

Chan L-H, Frey FA (2003) Lithium isotope geochemistry of the Hawaiian plume: results from the Hawaii Scientific Drilling Project and Koolau Volcano. Geochem Geophys Geosyst 4(3):8707. doi:10.1029/2002GC000365

Chan L-H, Edmond JM, Thompson G, Gillis K (1992) Lithium isotopic composition of submarine basalts: implications for lithium cycle in the oceans. Earth Planet Sci Lett 108:151–160. doi:10.1016/0012-821X(92)90067-6

Chan L-H, Alt JC, Teagle DAH (2002) Lithium and lithium isotope profiles through the upper oceanic crust: a study of seawater-basalt exchange at ODP Sites 504B and 896A. Earth Planet Sci Lett 201:187–201. doi:10.1016/S0012-821X(02)00707-0

Chan L-H, Leeman WP, Plank T (2006a) Lithium isotopic composition of marine sediments. Geochem Geophys Geosyst 7(6):Q06005. doi:10.1029/2005GC001202

Chan L-H, Savov IP, Ryan JG (2006b) Lithium isotope study of peridotite-slab fluid interactions in the Mariana forearc mantle wedge. EOS Trans AGU 87(36). Jt. Assemb. Suppl. Abstract V43A-03

Condie KC, Cox J, O'Reilly SY, Griffin WL, Kerrich R (2004) Distribution of high field strength and rare earth elements in mantle and lower crustal xenoliths from the southwestern United States: the role of grain-boundary phases. Geochim Cosmochim Acta 68:3919–3942. doi:10.1016/j.gca.2004.03.025

Coogan LA, Kasemann SA, Chakraborty S (2005) Rates of hydrothermal cooling of new oceanic upper crust derived from lithium-geospeedometry. Earth Planet Sci Lett 240:415–424. doi:10.1016/j.epsl.2005.09.020

Crank J (1975) The mathematics of diffusion. Clarendon Press, Oxford, p 414

Dick HJB, Bullen T (1984) Chromian spinel as a petrogenetic indicator in abyssal and alpine-type peridotites and spatially associated lavas. Contrib Mineral Petrol 86:54–76. doi:10.1007/BF00373711

Dick HJB, Natland JH (1996) Late-stage melt evolution and transport in the shallow mantle beneath the East Pacific Rise. In: Mével C, Gillis KM, Allan JF, Meyer PS (eds) Proceedings of the ocean drilling program, scientific results, vol 147, pp 103–134

Duggen S, Portnyagin M, Baker J, Ulfbeck D, Hoernle K, Garbe-Schönberg D, Grassineau N (2007) Drastic shift in lava geochemistry in the volcanic-front to rear-arc region of the Southern Kamchatkan subduction zone: evidence for the transition from slab surface dehydration to sediment melting. Geochim Cosmochim Acta 71:452–480. doi:10.1016/j.gca.2006.09.018

Eggins SM, Rudnick RL, McDonough WF (1998) The composition of peridotites and their minerals: a laser-ablation ICP-MS study. Earth Planet Sci Lett 154:53–71. doi:10.1016/S0012-821X(97)00195-7

Eiler JM, McInnes B, Valley JW, Graham CM, Stolper EM (1998) Oxygen isotope evidence for slab-derived fluids in the sub-arc mantle. Nature 393:777–781. doi:10.1038/31679

Eiler J, Schiano P, Valley JW, Kita NT, Stolper E (2007) Oxygen-isotope and trace element constraints on the origins of silica-rich melts in the subarc mantle. Geochem Geophys Geosyst 8(9):Q09012. doi:10.1029/2006GC001503

Elliott T (2003) Tracers of the slab. In: Eiler J (ed) Inside the subduction factory. Geophysical monograph, vol 138. American Geophysical Union, Washington DC, pp 23–45

Elliott T, Jeffcoate A, Bouman C (2004) The terrestrial Li isotope cycle: light-weight constraints on mantle convection. Earth Planet Sci Lett 220:231–245. doi:10.1016/S0012-821X(04)00096-2

Elliott T, Thomas A, Jeffcoate A, Niu Y (2006) Lithium isotope evidence for subduction-enriched mantle in the source of mid-ocean-ridge basalts. Nature 443:565–568. doi:10.1038/nature05144

Ernst WG (1999) Hornblende, the continent maker—evolution of H_2O during circum-Pacific subduction versus continental collision. Geology 27:675–678. doi:10.1130/0091-7613(1999)027<0675:HTCMEO>2.3.CO;2

Falloon TJ, Danyushevshy LV (2000) Melting of refractory mantle at 1.5, 2 and 2.5 GPa under anhydrous and H_2O-undersaturated conditions: implications for the petrogenesis of high-Ca boninites and the influence of subduction components on mantle melting. J Petrol 41:257–283. doi:10.1093/petrology/41.2.257

Gaetani GA, Kent AJR, Grove TL, Hutcheon ID, Stolper EM (2003) Mineral/melt partitioning of trace elements during hydrous peridotite partial melting. Contrib Mineral Petrol 145:391–405. doi:10.1007/s00410-003-0447-0

Gao Y, Casey JF, Snow JE (2008) Isotopic fractionation of Li during cooling of mantle peridotite from Gakkel Ridge. EOS Trans AGU 89(53). Fall Meet. Suppl. Abstract V32A-03

Giletti BJ, Shanahan TM (1997) Alkali diffusion in plagioclase feldspar. Chem Geol 139:3–20. doi:10.1016/S0009-2541(97)00026-0

Gill JB (1981) Orogenic andesites and plate tectonics. Springer, Berlin, p 390

Glaser SM, Foley SF, Gunther D (1999) Trace element compositions of minerals in garnet and spinel peridotite xenoliths from the Vitim volcanic field, Transbaikalia, eastern Siberia. Lithos 48:263–285. doi:10.1016/S0024-4937(99)00032-8

Gorbatov A, Kostoglodov V, Suarez G, Gordeev E (1997) Seismicity and structure of the Kamchatka subduction zone. J Geophys Res 102:17883–17898. doi:10.1029/96JB03491

Green TH, Adam J (2003) Experimentally-determined trace element characteristics of aqueous fluid from partially dehydrated mafic oceanic crust at 3.0 GPa, 650–700°C. Eur J Mineral 15:815–830. doi:10.1127/0935-1221/2003/0015-0815

Green TH, Blundy JD, Adam J, Yaxley GM (2000) SIMS determination of trace element partition coefficients between garnet, clinopyroxene and hydrous basaltic liquids at 2–7.5 GPa and

1080–1200°C. Lithos 53:165–187. doi:10.1016/S0024-4937(00)00023-2
Halama R, McDonough WF, Rudnick RL, Keller J, Klaudius J (2007) The Li isotopic composition of Oldoinyo Lengai: nature of the mantle sources and lack of isotopic fractionation during carbonatite petrogenesis. Earth Planet Sci Lett 254:77–89. doi:10.1016/j.epsl.2006.11.022
Halama R, McDonough WF, Rudnick RL, Bell K (2008) Tracking the lithium isotopic evolution of the mantle using carbonatites. Earth Planet Sci Lett 265:726–742. doi:10.1016/j.epsl.2007.11.007
Hart SR, Blusztajn J, Dick HJB, Meyer PS, Muehlenbachs K (1999) The fingerprint of seawater circulation in a 500-meter section of ocean crust gabbros. Geochim Cosmochim Acta 63:4059–4080. doi:10.1016/S0016-7037(99)00309-9
Hawkesworth CJ, Gallagher K, Hergt JM, McDermott F (1993) Mantle and slab contributions in arc magmas. Annu Rev Earth Planet Sci 21:175–204
Heinrich W, Besch T (1992) Thermal history of the upper mantle beneath a young back-arc extensional zone: ultramafic xenoliths from San Luis Potosí, Central Mexico. Contrib Mineral Petrol 111:126–142. doi:10.1007/BF00296583
Hellebrand E, Snow JE, Dick HJB, Hofmann AW (2001) Coupled major and trace element as indicators of the extent of melting in mid-ocean ridge peridotites. Nature 410:677–681. doi:10.1038/35070546
Hickey RL, Frey FA (1982) Geochemical characteristics of boninite series volcanics: implications for their source. Geochim Cosmochim Acta 46:2099–2115. doi:10.1016/0016-7037(82)90188-0
Hiraga T, Anderson IM, Kohlstedt DL (2004) Grain boundaries as reservoirs of incompatible elements in the Earth's mantle. Nature 427:699–703. doi:10.1038/nature02259
Hofmann AW (2003) Sampling mantle heterogeneity through oceanic basalts: isotopes and trace elements. In: Carlson RW (ed) Treatise on geochemistry, vol 2: the mantle and core. Elsevier-Pergamon, Oxford, pp 61–101
Ionov DA, Hofmann AW (1995) Nb-Ta-rich mantle amphiboles and micas: implications for subduction-related metasomatic trace element fractionations. Earth Planet Sci Lett 131:341–356. doi:10.1016/0012-821X(95)00037-D
Ionov DA, Seitz H-M (2008) Lithium abundances and isotopic compositions in mantle xenoliths from subduction and intra-plate settings: mantle sources vs. eruption histories. Earth Planet Sci Lett 266:316–331. doi:10.1016/j.epsl.2007.11.020
Ionov DA, Bodinier J-L, Mukasa SB, Zanetti A (2002) Mechanisms and sources of mantle metasomatism: major and trace element compositions of peridotite xenoliths from Spitsbergen in the context of numerical modelling. J Petrol 43:2219–2259. doi:10.1093/petrology/43.12.2219
Ishimaru S, Arai S (2008a) Nickel enrichment in mantle olivine beneath a volcanic front. Contrib Mineral Petrol 156:119–131. doi:10.1007/s00410-007-0277-6
Ishimaru S, Arai S (2008b) Calcic amphiboles in peridotite xenoliths from Avacha volcano, Kamchatka, and their implications for metasomatic conditions in the mantle wedge. In: Coltorti M, Grégoire M (eds) Metasomatism in continental and oceanic lithospheric mantle. Geol Soc Lond Spec Publ 293:35–55
Ishimaru S, Arai S (2008c) Highly silicic glasses in peridotite xenoliths from Avacha volcano, Kamchatka arc; implications for melting and metasomatism within the sub-arc mantle. Lithos. doi:10.1016/j.lithos.2008.07.005
Ishimaru S, Arai S, Ishida Y, Shirasaka M, Okrugin VM (2007) Melting and multi-stage metasomatism in the mantle wedge beneath a frontal arc inferred from highly depleted peridotite xenoliths from the Avacha volcano, Southern Kamchatka. J Petrol 48:395–433. doi:10.1093/petrology/egl065
James RH, Palmer MR (2000) The lithium isotope composition of international rock standards. Chem Geol 166:319–326. doi:10.1016/S0009-2541(99)00217-X
Jeffcoate AB, Elliott T, Thomas A, Bouman C (2004) Precise, small sample size determinations of lithium isotopic compositions of geological reference materials and modern seawater by MC-ICP-MS. Geostand Geoanal Res 28:161–172. doi:10.1111/j.1751-908X.2004.tb01053.x
Jeffcoate AB, Elliott T, Kasemann SA, Ionov D, Cooper K, Brooker R (2007) Li isotope fractionation in peridotites and mafic melts. Geochim Cosmochim Acta 71:202–218. doi:10.1016/j.gca.2006.06.1611
Johnson KTM, Dick HJB, Shimizu N (1990) Melting in the Oceanic Upper Mantle: an ion microprobe study of diopsides in abyssal peridotites. J Geophys Res 95:2661–2678. doi:10.1029/JB095iB03p02661
Kelemen PB, Hart SR, Bernstein S (1998) Silica enrichment in the continental upper mantle via melt/rock reaction. Earth Planet Sci Lett 164:387–406. doi:10.1016/S0012-821X(98)00233-7
Kelemen PB, Hanghøj K, Greene AR (2003) One view of the Geochemistry of subduction-related magmatic arcs, with an emphasis on primitive andesite and lower crust. In: Rudnick RL (ed) Treatise on geochemistry, vol 3: the crust. Elsevier-Pergamon, Oxford, pp 593–659
Kelley KA, Plank T, Ludden J, Staudigel H (2003) Composition of altered oceanic crust at ODP sites 801 and 1149. Geochem Geophys Geosyst 4(6):8910. doi:10.1029/2002GC000435
Kepezhinskas P, Defant MJ (1996) Contrasting styles of mantle metasomatism above subduction zones: constraints from ultramafic xenoliths in Kamchatka. In: Bebout GE, Scholl DW, Kirby SH, Platt JP (eds) Subduction: top to bottom. Geophys Monogr 96:307–314
Kepezhinskas P, Defant MJ (2001) Nonchondritic Pt/Pd ratios in arc mantle xenoliths: evidence for platinum enrichment in depleted island-arc mantle sources. Geology 29:851–854. doi:10.1130/0091-7613(2001)029<0851:NPPRIA>2.0.CO;2
Kepezhinskas P, Defant MJ, Drummond MS (1995) Na metasomatism in the island-arc mantle by slab melt-peridotite interaction: evidence from mantle xenoliths in the North Kamchatka Arc. J Petrol 36:1505–1527
Kepezhinskas P, Defant MJ, Drummond MS (1996) Progressive enrichment of island arc mantle by melt-peridotite interaction inferred from Kamchatka xenoliths. Geochim Cosmochim Acta 60:1217–1229. doi:10.1016/0016-7037(96)00001-4
Kepezhinskas P, McDermott F, Defant MJ, Hochstaedter A, Drummond MS, Hawkesworth CJ, Koloskov A, Maury R, Bellon H (1997) Trace element and Sr-Nd-Pb isotopic constraints on a three-component model of Kamchatka Arc petrogenesis. Geochim Cosmochim Acta 61:577–600. doi:10.1016/S0016-7037(96)00349-3
Kepezhinskas P, Defant MJ, Widom E (2002) Abundance and distribution of PGE and Au in the island-arc mantle: implications for sub-arc metasomatism. Lithos 2002:113–128. doi:10.1016/S0024-4937(01)00073-1
Keppler H (1996) Constraints from partitioning experiments on the composition of subduction-zone fluids. Nature 380:237–240. doi:10.1038/380237a0
Kessel R, Schmidt MW, Ulmer P, Pettke T (2005) Trace element signature of subduction-zone fluids, melts and supercritical liquids at 120–180 km depth. Nature 437:724–727. doi:10.1038/nature03971
Koloskov AV, Puzankov MY, Pirozhkova ES (2001) Ultramafic inclusions in island arc basaltoids: the problem of the composition and genesis of the transitional "crust–mantle mixture" layer in island arc systems. In: Geodinamika i vulkanizm Kurilo-Kamchatskoi ostrovoduzhnoi sistemy (Geodynamics and

Volcanism of the Kuril–Kamchatka Island Arc System), IVGiG DVO RAN, Petropavlovsk-Kamchatskii, pp 123–152

Lee C-T, Harbert A, Leeman WP (2007) Extension of lattice strain theory to mineral/mineral rare-earth element partitioning: an approach for assessing disequilibrium and developing internally consistent partition coefficients between olivine, orthopyroxene, clinopyroxene and basaltic melt. Geochim Cosmochim Acta 71:481–496. doi:10.1016/j.gca.2006.09.014

Levin V, Park J, Brandon M, Lees J, Peyton V, Gordeev E, Ozerov A (2002) Crust and upper mantle of Kamchatka from teleseismic receiver functions. Tectonophysics 358:233–265. doi:10.1016/S0040-1951(02)00426-2

Luhr JF, Aranda-Gómez JJ (1997) Mexican peridotite xenoliths and tectonic terranes: correlations among vent location, texture, temperature, pressure, and oxygen fugacity. J Petrol 38:1075–1112. doi:10.1093/petrology/38.8.1075

Magna T, Wiechert UH, Halliday AN (2004) Low-blank isotope ratio measurement of small samples of lithium using multiple-collector ICPMS. Int J Mass Spectrom 239:67–76. doi:10.1016/j.ijms.2004.09.008

Magna T, Wiechert U, Halliday AN (2006) New constraints on the lithium isotope compositions of the Moon and terrestrial planets. Earth Planet Sci Lett 243:336–353. doi:10.1016/j.epsl.2006.01.005

Manea VC, Manea M (2007) Thermal models beneath Kamchatka and the Pacific plate rejuvenation from a mantle plume impact. In: Eichelberger J, Izbekov P, Ruppert N, Gordeev E, Lees J (eds) Volcanism and tectonics of the Kamchatka peninsula and adjacent arcs. Geophys Monogr 172:77–90

Marks M, Halama R, Wenzel T, Markl G (2004) Trace element variations in clinopyroxene and amphibole from alkaline to peralkaline syenites and granites: implications for mineral-melt trace element partitioning. Chem Geol 211:185–215. doi:10.1016/j.chemgeo.2004.06.032

Marks M, Rudnick RL, McCammon C, Vennemann TW, Markl G (2007) Arrested kinetic Li isotope fractionation at the margin of the Ilímaussaq complex, South Greenland: evidence for open-system processes during final cooling of peralkaline igneous rocks. Chem Geol 246:207–230. doi:10.1016/j.chemgeo.2007.10.001

Marschall HR, Altherr R, Ludwig T, Kalt A, Gméling K, Kasztovszky Z (2006) Partitioning and budget of Li, Be and B in high-pressure metamorphic rocks. Geochim Cosmochim Acta 70:4750–4769. doi:10.1016/j.gca.2006.07.006

Marschall HR, Pogge von Strandmann PAE, Seitz H-M, Elliott T, Niu Y (2007) The lithium isotopic composition of orogenic eclogites and deep subducted slabs. Earth Planet Sci Lett 262:563–580. doi:10.1016/j.epsl.2007.08.005

McDonough WF, Sun S-S (1995) The composition of the Earth. Chem Geol 120:223–253. doi:10.1016/0009-2541(94)00140-4

Münker C, Wörner G, Yogodzinski G, Churikova T (2004) Behaviour of high field strength elements in subduction zones: constraints from Kamchatka-Aleutian arc lavas. Earth Planet Sci Lett 224:275–293. doi:10.1016/j.epsl.2004.05.030

Müntener O, Kelemen PB, Grove TL (2001) The role of H_2O during crystallization of primitive arc magmas under uppermost mantle conditions and genesis of igneous pyroxenites: an experimental study. Contrib Mineral Petrol 141:643–658

Nishio Y, Nakai S, Yamamoto J, Sumino H, Matsumoto T, Prikhod'ko VS, Arai S (2004) Lithium isotopic systematics of the mantle-derived ultramafic xenoliths: implications for EM1 origin. Earth Planet Sci Lett 217:245–261. doi:10.1016/S0012-821X(03)00606-X

Nixon PH (1987) Mantle xenoliths. Wiley, New York, p 844

Nizkous IV, Sanina IA, Kissling E, Gontovaya LI (2006) Velocity properties of the lithosphere in the ocean-continent transition zone in the Kamchatka region from seismic tomography data. Izvestiya. Phys Solid Earth 42:286–296. doi:10.1134/S1069351306040033

O'Neill HSC (1981) The transition between spinel lherzolite and garnet lherzolite, and its use as a geobarometer. Contrib Mineral Petrol 77:185–194. doi:10.1007/BF00636522

Osipenko AB (2003) New data on boninite magmatism of Eastern Kamchatka. Dokl Earth Sci 391A:892–895

Ottolini L, Le Fèvre B, Vannucci R (2004) Direct assessment of mantle boron and lithium contents and distribution by SIMS analyses of peridotite minerals. Earth Planet Sci Lett 228:19–36. doi:10.1016/j.epsl.2004.09.027

Ozawa K (1994) Melting and melt segregation in the mantle wedge above a subduction zone: evidence from the chromite-bearing peridotites of the Miyamori ophiolite complex, northeastern Japan. J Petrol 35:647–678

Parkinson IJ, Hammond SJ, James RH, Rogers NW (2007) High-temperature lithium isotope fractionation: insights from lithium isotope diffusion in magmatic systems. Earth Planet Sci Lett 257:609–621. doi:10.1016/j.epsl.2007.03.023

Pearson DG, Canil D, Shirey SB (2003) Mantle samples included in volcanic rocks: xenoliths and diamonds. In: Carlson RW (ed) Treatise on geochemistry, vol 2: the mantle and core. Elsevier-Pergamon, Oxford, pp 171–275

Plank T, Langmuir CH (1998) The chemical composition of subducting sediment and its consequences for the crust and mantle. Chem Geol 145:325–394. doi:10.1016/S0009-2541(97)00150-2

Portnyagin M, Hoernle K, Avdeiko G, Hauff F, Werner R, Bindeman I, Uspensky V, Garbe-Schönberg D (2005) Transition from arc to oceanic magmatism at the Kamchatka-Aleutian junction. Geology 33:23–28. doi:10.1130/G20853.1

Prouteau G, Scaillet B, Pichavant M, Maury R (2001) Evidence for mantle metasomatism by hydrous silicic melts derived from subducted oceanic crust. Nature 410:197–200. doi:10.1038/35065583

Qi HP, Taylor PDP, Berglund M, De Bievre P (1997) Calibrated measurements of the isotopic composition and atomic weight of the natural Li isotopic reference material IRMM-016. Int J Mass Spectrom Ion Process 171:263–268. doi:10.1016/S0168-1176(97)00125-0

Ranero CR, Phipps Morgan J, McIntosh K, Reichert C (2003) Bending-related faulting and mantle serpentinization at the Middle America trench. Nature 425:367–373. doi:10.1038/nature01961

Rehkämper M, Hofmann AW (1997) Recycled ocean crust and sediment in Indian Ocean MORB. Earth Planet Sci Lett 147:93–106. doi:10.1016/S0012-821X(97)00009-5

Renkin ML, Sclater JG (1988) Depth and age in the North Pacific. J Geophys Res 93(B4):2919–2935. doi:10.1029/JB093iB04p02919

Richter FM, Davis AM, DePaolo DJ, Watson EB (2003) Isotope fractionation by chemical diffusion between molten basalt and rhyolite. Geochim Cosmochim Acta 67:3905–3923. doi:10.1016/S0016-7037(03)00174-1

Rudnick RL, Ionov D (2007) Lithium elemental and isotopic disequilibrium in minerals from peridotite xenoliths from far-east Russia: product of recent melt/fluid-rock reaction. Earth Planet Sci Lett 256:278–293. doi:10.1016/j.epsl.2007.01.035

Rudnick RL, Tomascak PB, Heather BN, Gardner LR (2004) Extreme lithium isotopic fractionation during continental weathering revealed in saprolites from South Carolina. Chem Geol 212:45–57. doi:10.1016/j.chemgeo.2004.08.008

Ryan JG, Kyle PR (2004) Lithium abundance and lithium isotope variations in mantle sources: insights from intraplate volcanic rocks from Ross Island and Marie Byrd Land (Antarctica) and

other oceanic islands. Chem Geol 212:125–142. doi:10.1016/j.chemgeo.2004.08.006

Ryan JG, Langmuir CH (1987) The systematics of lithium abundances in young volcanic rocks. Geochim Cosmochim Acta 51:1727–1741. doi:10.1016/0016-7037(87)90351-6

Saha A, Basu AR, Jacobsen SB, Poreda RJ, Yin Q-Z, Yogodzinski GM (2005) Slab devolatilization and Os and Pb mobility in the mantle wedge of the Kamchatka arc. Earth Planet Sci Lett 236:182–194. doi:10.1016/j.epsl.2005.05.018

Savov IP, Ryan JG, Chan L-H, D'Antonio M, Mottl M, Fryer P, Party OLS (2002) Geochemistry of serpentinites from the S. Chamorro Seamount, ODP leg 195, site 1200, Mariana Forearc—implications for recycling at subduction zones. Geochim Cosmochim Acta 66(Suppl 1):A670

Savov IP, Ryan JG, D'Antonio M, Kelley K, Mattie P (2005) Geochemistry of serpentinized peridotites from the Mariana Forearc Conical Seamount, ODP leg 125: implications for the elemental recycling at subduction zones. Geochem Geophys Geosyst 6(4):Q04J15. doi:10.1029/2004GC000777

Savov IP, Ryan JG, D'Antonio M, Fryer P (2007) Shallow slab fluid release across and along the Mariana arc-basin system: Insights from geochemistry of serpentinized peridotites from the Mariana fore arc. J Geophys Res 112:B09205. doi:09210.01029/02006JB004749

Schmidt MW, Poli S (2003) Generation of mobile components during subduction of oceanic crust In: Rudnick RL (ed) Treatise on geochemistry, vol 3: the crust. Elsevier-Pergamon, Oxford, pp 567–591

Schwartz S, Allemand P, Guillot S (2001) Numerical model of the effect of serpentinites on the exhumation of eclogitic rocks: insights from the Monviso ophiolite massif. Tectonophysics 342:193–206. doi:10.1016/S0040-1951(01)00162-7

Seitz H-M, Woodland AB (2000) The distribution of lithium in peridotitic and pyroxenitic mantle lithologies—an indicator of magmatic and metasomatic processes. Chem Geol 166:47–64. doi:10.1016/S0009-2541(99)00184-9

Seitz H-M, Brey GP, Lahaye Y, Durali S, Weyer S (2004) Lithium isotopic signatures of peridotite xenoliths and isotopic fractionation at high temperature between olivine and pyroxenes. Chem Geol 212:163–177. doi:10.1016/j.chemgeo.2004.08.009

Seitz H-M, Brey GP, Weyer S, Durali S, Ott U, Münker C, Mezger K (2006) Lithium isotope compositions of Martian and lunar reservoirs. Earth Planet Sci Lett 245:6–18. doi:10.1016/j.epsl.2006.03.007

Shang CK, Satir M, Nsifa EN, Liégois J-P, Siebel W, Taubald H (2007) Archaean high-K granitoids produced by remelting of earlier tonalite-trondhjemite-granodiorite (TTG) in the Sangmelima region of the Ntem complex of the Congo craton, southern Cameroon. Int J Earth Sci 96:817–841. doi:10.1007/s00531-006-0141-3

Singer BS, Jicha BR, Leeman WP, Rogers NW, Thirlwall MF, Ryan J, Nicolaysen K (2007) Along-strike trace element and isotopic variation in Aleutian Island arc basalt: subduction melts sediments and dehydrates serpentine. J Geophys Res 112:B06206. doi:06210.01029/02006JB004897

Stalder R, Foley SF, Brey GP, Horn I (1998) Mineral-aqueous fluid partitioning of trace elements at 900-1200°C and 3.0–5.7 GPa: new experimental data for garnet, clinopyroxene, and rutile, and implications for mantle metasomatism. Geochim Cosmochim Acta 62:1781–1801. doi:10.1016/S0016-7037(98)00101-X

Stern RJ, Morris J, Bloomer SH, Hawkins JW (1991) The source of the subduction component in convergent margin magmas: trace element and radiogenic isotope evidence from Eocene boninites, Mariana forearc. Geochim Cosmochim Acta 55:1467–1481. doi:10.1016/0016-7037(91)90321-U

Straub SM, Layne GD (2003) Decoupling of fluids and fluid-mobile elements during shallow subduction: evidence from halogen-rich andesite melt inclusions from the Izu arc volcanic front. Geochem Geophys Geosyst 4(7):9003. doi:10.1029/2002GC000349

Sun S-S, McDonough WF (1989) Chemical and isotopic systematics of oceanic basalts: implications for mantle composition and processes. In: Saunders AD, Norry MJ (eds) Magmatism in the Ocean Basins. Geol Soc Lond Spec Publ 42:313–345

Tamura A, Arai S (2006) Harzburgite-dunite-orthopyroxenite suite as a record of supra-subduction zone setting for the Oman ophiolite mantle. Lithos 90:43–56. doi:10.1016/j.lithos.2005.12.012

Teng F-Z, McDonough WF, Rudnick RL, Dalpé C, Tomascak PB, Chappell BW, Gao S (2004) Lithium isotopic composition and concentration of the upper continental crust. Geochim Cosmochim Acta 68:4167–4178. doi:10.1016/j.gca.2004.03.031

Teng F-Z, McDonough WF, Rudnick RL, Walker RJ (2006) Diffusion-driven extreme lithium isotopic fractionation in country rocks of the Tin Mountain pegmatite. Earth Planet Sci Lett 243:701–710. doi:10.1016/j.epsl.2006.01.036

Tomascak PB, Tera F, Helz RT, Walker RJ (1999) The absence of lithium isotope fractionation during basalt differentiation: new measurements by multicollector sector ICP-MS. Geochim Cosmochim Acta 63:907–910. doi:10.1016/S0016-7037(98)00318-4

Tomascak PB, Ryan JG, Defant MJ (2000) Lithium isotope evidence for light element decoupling in the Panama subarc mantle. Geology 28:507–510. doi:10.1130/0091-7613(2000)28<507:LIEFLE>2.0.CO;2

Tomascak PB, Widom E, Benton LD, Goldstein SL, Ryan JG (2002) The control of lithium budgets in island arcs. Earth Planet Sci Lett 196:227–238. doi:10.1016/S0012-821X(01)00614-8

Tomascak PB, Langmuir CH, le Roux PJ, Shirey SB (2008) Lithium isotopes in global mid-ocean ridge basalts. Geochim Cosmochim Acta 72:1626–1637. doi:10.1016/j.gca.2007.12.021

Turner S, McDermott F, Hawkesworth C, Kepezhinskas P (1998) A U-series study of lavas from Kamchatka and the Aleutians: constraints on source composition and melting processes. Contrib Mineral Petrol 133:217–234. doi:10.1007/s004100050449

van Orman JA, Grove TL, Shimizu N (2001) Rare earth element diffusion in diopside: influence of temperature, pressure, and ionic radius, and an elastic model for diffusion in silicates. Contrib Mineral Petrol 141:687–703

Widom E, Kepezhinskas P, Defant MJ (2003) The nature of metasomatism in the sub-arc mantle wedge: evidence from Re-Os isotopes in Kamchatka peridotite xenoliths. Chem Geol 196:283–306. doi:10.1016/S0009-2541(02)00417-5

Wilson AH (1982) The geology of the Great 'Dyke', Zimbabwe: the ultramafic rocks. J Petrol 23:240–292

Wunder B, Meixner A, Romer RL, Heinrich W (2006) Temperature-dependent isotopic fractionation on lithium between clinopyroxene and high-pressure hydrous fluids. Contrib Mineral Petrol 151:112–120. doi:10.1007/s00410-005-0049-0

Wunder B, Meixner A, Romer RL, Feenstra A, Schettler G, Heinrich W (2007) Lithium isotope fractionation between Li-bearing staurolite, Li-mica and aqueous fluids: an experimental study. Chem Geol 238:277–290. doi:10.1016/j.chemgeo.2006.12.001

Zack T, Tomascak PB, Rudnick RL, Dalpé C, McDonough WF (2003) Extremely light Li in orogenic eclogites: the role of isotope fractionation during dehydration in subducted oceanic crust. Earth Planet Sci Lett 208:279–290. doi:10.1016/S0012-821X(03)00035-9

Zipfel J, Wörner G (1992) Four- and five-phase peridotites from a continental rift system: evidence for upper mantle uplift and cooling at the Ross Sea margin (Antarctica). Contrib Mineral Petrol 111:24–36. doi:10.1007/BF00296575